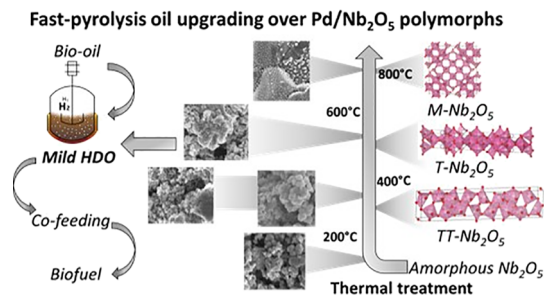


Investigation of Nb₂O₅ and Its Polymorphs as Catalyst Supports for Pyrolysis Oil Upgrading through Hydrodeoxygenation

Mariana Myriam Campos Fraga,* Jonas Vogt, Bruno Lacerda de Oliveira Campos, Caroline Carriel Schmitt, Klaus Raffelt, and Nicolaus Dahmen

ABSTRACT: Mild catalytic hydrogenation is an interesting process to upgrade and stabilize raw fast-pyrolysis oil, allowing higher ratios of bio-oil to be coprocessed in conventional refineries. In the search for hydrodeoxygenation (HDO) catalysts with high activity, high selectivity, and long-term stability, Nb₂O₅-supported catalysts are stressed owing to their water-resistant acid sites. Due to the Nb₂O₅ polymorphism, its properties such as acidity, morphology, and crystalline structure are adjustable. This study evaluated the suitability of Nb₂O₅ as a catalyst support and the impact of its different polymorphs on the upgrading of pyrolysis oil. Four different Nb₂O₅ polymorphs were prepared by thermal treatment of niobic acid, and nanostructured Nb₂O₅ was prepared by hydrothermal synthesis with niobium oxalate. The supports were wet impregnated with Pd (1 wt %) and applied for the upgrading of the light phase of beech wood fast-pyrolysis oil (FPO-LP) in a batch reactor, pressurized at 80 bar H₂ (room temperature), and heated to 250 °C for 2 hours. The activity and selectivity of catalysts and the dominant reaction pathways were addressed in terms of upgraded product properties (elemental composition, water content, functional groups via ¹H-NMR, and chemical composition via GC-MS/FID), H₂ consumption, generated gases, deoxygenation degree, and catalyst deactivation via coke formation. Nb₂O₅ showed outstanding potential as a catalyst support for FPO-LP HDO, taking into account the improved properties of the upgraded oil, such as higher carbon content and lower water and oxygen contents. The polymorphs without thermal treatment (Pd/TT&A-Nb₂O₅) or with a low-temperature thermal treatment (Pd/TT&A-Nb₂O₅) presented higher activity than the one obtained at high temperature (Pd/M&T-Nb₂O₅). The high stability of the Pd/A-Nb₂O₅ was demonstrated by regeneration and re-use. Finally, the nanostructured TT-Nb₂O₅ presented a remarkable activity toward hydrogenation and hydrogenolysis, owing to its higher acidity and surface area, resulting in the most improved oil.



1. INTRODUCTION

Recently, the search for alternative energy sources has received considerable attention, especially for the transportation sector. Biomass has been pointed out as a promising source to reduce the dependence on fossil fuels and, consequently, to improve the energy supply security of several countries. Lignocellulosic biomass (e.g., from energy crops, agricultural residues, and forestry residues) can be used to provide renewable fuels that do not compete with food crops.¹ Notwithstanding the environmental, political, and economic benefits of the lignocellulosic biomass, the challenges associated with processing such complex and varied molecules derived from this kind of biomass tend to hinder its application. In this context, the biorefinery concept seems to embrace the task with a “sustainable processing of biomass into a spectrum of marketable products and energy”.² In an equivalent version to petroleum refinery, several biorefinery concepts propose the production of sustainable fuels from fast-pyrolysis bio-oil.³ Fast-pyrolysis takes advantage of the thermal instability of biomass when submitted to high temperatures in the absence

of oxygen for short residence time to produce bio-oil in a maximized yield. Despite the fact that slow-pyrolysis is an ancient technique, the interest in the pyrolysis liquid product (bio-oil) was intensified only after the oil crisis (1970s). In the last 30 years, the fast-pyrolysis process has been intensively improved, and its direct uses are as boiler fuel and in heavy-duty engines.⁴ The restricted number of direct applications of bio-oil comes from its properties: high water (15–50 wt %), several oxygenated molecules classes (e.g., carboxylic acids, ketones, alcohols, esters, phenols, and guaiacols), high acidity, high instability, high coking tendency due to re-polymerization issues, low volatility, and low higher heating value (HHV = 16–19 MJ kg⁻¹).⁵

The integration of bio-oil into the well-established petrochemical refinery has been pointed out as a way to ease the early-stage transition toward a more bio-based economy.^{6,7} The feasibility of coprocessing raw fast-pyrolysis oil with refinery fractions has already been demonstrated using segregated stream injections on pilot FCC units.^{8,9} In 2021, Preem (Lysekil, Sweden) announced plans to coprocess 24,000 tons of bio-oil per year produced by Pyrocell (Gävle, Sweden) with vacuum gas oil (VGO) in its fluid catalytic cracker (FCC) unit.¹⁰ Nonetheless, the ratio of raw bio-oil to petroleum streams is still limited to 5–10 wt %, since higher bio-oil ratios would lead to coking, catalyst deactivation, and deterioration of gasoline yields.⁹ Hence, in order to expand the bio-oil amount in cofeeding plants, a previous upgrade of the bio-oil via partial hydrodeoxygenation (HDO) is a promising alternative.¹¹ In this regard, the required bio-oil properties and, consequently, the minimum upgrading extension (HDO intensity) to enable coprocessing at large oil ratios are still unclear.¹² Some relevant parameters to describe the quality of the upgraded oil are oxygen content, H/C, $H/C_{\text{effective}}$, molecular weight, miscibility, and coking tendency.^{13–15}

The catalyst is one of the key factors for the bio-oil upgrading through HDO. In the search for high activity, selectivity, and stability, several catalyst compositions have been evaluated for bio-oil HDO.^{16,17} Within bifunctional catalysts, Nb_2O_5 has received attention as a catalyst support for HDO of biomass streams owing to its water-resistant acid sites.¹⁸ Nb_2O_5 as a support for Pd, Ru, Co, and Ni has led to a remarkable increase in activity, selectivity, and stability in comparison to reference supports. In a previous study from our group, the application of Nb_2O_5 as a catalyst support for bio-oil HDO has been demonstrated.¹⁹

Nb_2O_5 can be obtained in at least 15 different phases, the so-called polymorphs. Brauer was the pioneer on the study of Nb_2O_5 polymorphs.²⁰ In 1941, he analyzed three Nb_2O_5 phases that he named based on their crystallization temperature range: *T* (from German *tief*, i.e., low), *M* (from German *mittel*, i.e., middle), and *H* (from German *hoch*, i.e., high). Later on, in 1966, Schäfer and colleagues compiled several Nb_2O_5 polymorphs and identified them in a systematic way.²¹ For that, while some polymorphs were identified based on their crystallization temperatures, others were named after their particle shapes. Following studies continued identifying new polymorphs and differentiating some obtained at similar temperatures.^{22,23} However, this systematic identification was not followed unanimously by the scientific community, and later some of the studies restricted the polymorph categorization into two big groups: high-temperature polymorphs and low-temperature polymorphs.²⁴

Schäfer et al.²¹ considered the octahedral elements decisive to the multiplicity of Nb_2O_5 phases. They stated that the broad range of Nb_2O_5 polymorphs comes from the several combinations of various octahedral linkages that satisfy the stoichiometric O/Nb ratio of 2.5. The obtainment of a specific polymorph is determined through the starting materials, impurities, and thermal treatments, as well through other synthesis parameters, and they vary largely in terms of properties as pointed in the next paragraphs:

1.1. Niobic Acid ($Nb_2O_5 \cdot nH_2O$) and Amorphous Nb_2O_5 . The amorphous Nb_2O_5 hydrate ($Nb_2O_5 \cdot nH_2O$), also known as niobic acid, is a white solid with a high acid strength (corresponding to 70% acid strength of H_2SO_4).²⁵ Its acidity comes from the formation of strong Brønsted and Lewis acids

by H^+ generation from H_2O on exposed Nb^{5+} . It is regarded as a unique solid acid due its acidity in spite of presence of water, an advantage over zeolites for example.^{25,26} The $Nb_2O_5 \cdot nH_2O$ is mainly composed of distorted NbO_6 octahedra and NbO_4 tetrahedra (Figure 1). The Brønsted acid sites come from the

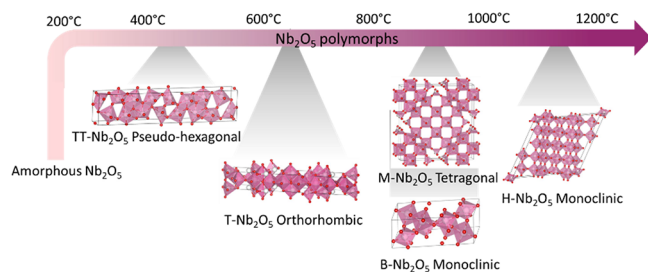


Figure 1. Nb_2O_5 phase transition to polymorphs TT- Nb_2O_5 (CCDC 2103847), T- Nb_2O_5 (ICSD 1840), M (COD 1528723), B (COD 1528678), and H- Nb_2O_5 (ICSD 29). The crystal structures were drawn with Vesta 3 software.²⁷

surface OH groups in the presence of the highly polarized Nb–O bonds from the distorted polyhedrons. In turn, the water-tolerant Lewis acid sites are generated on NbO_4 tetrahedra that still have effective positive charges even after the formation of the adducts $NbO_4 \cdot H_2O$.

1.2. TT- Nb_2O_5 . The TT polymorph, first mentioned by Frevel and Rinn,²⁸ is reported as one of the low-temperature phases of Nb_2O_5 . In the beginning, the TT-phase was accounted as a less crystalline form of T- Nb_2O_5 stabilized by impurities.²⁹ Nonetheless, Weissman et al.³⁰ refuted this hypothesis through HRTEM images showing that TT was a distinct well crystallized structure similar to the T- Nb_2O_5 . The exact temperature in which this phase transition from amorphous to TT happens depends on several factors.²² The TT structure has the highest number of oxygen vacancies of all polymorphs and, consequently, the highest degree of polyhedral distortion.³¹ The crystalline structure of the TT, first pointed out as a pseudo-hexagonal unit cell,²⁸ is still under intense debate due to its complex atom organization.³² In agreement with Frevel and Rinn,²⁸ Gomes and Mohallem³² recently elucidated the TT structure with a disordered pseudo-hexagonal unit cell that converges to a monoclinic system, forming an orthorhombic superlattice structure that is similar to the T-phase.

1.3. T- Nb_2O_5 . The T phase was one of the polymorphs already mentioned by Brauer in 1941. It has an orthorhombic crystal structure, in which the atoms are organized in distorted octahedral and pentagonal bipyramids.³¹ According to Ko and Weissman,²² the discrimination between T and TT phases is not trivial, although it may be done through X-ray diffraction (XRD) under ideal circumstances. Consequently, several studies do not differ between the low-temperature phases of Nb_2O_5 .^{24,33}

1.4. M- Nb_2O_5 . The M phase is one of the high-temperature forms of Nb_2O_5 .²² It has a tetragonal crystal structure and it is usually detected together with H- Nb_2O_5 . It presents similar XRD patterns to the B and H polymorphs.

1.5. B- Nb_2O_5 . The polymorph B-phase is formed at intermediate temperatures (700–900 °C) with monoclinic structure. The name comes from its characteristic bladed crystal habit with rutile-like ribbons of edge-sharing NbO_6 octahedra.²³

1.6. H-Nb₂O₅. The H phase is the easiest polymorph to obtain. It is formed at high temperatures starting from any Nb₂O₅ polymorph.²³ It is the thermodynamically most stable phase and presents a monoclinic structure.³⁴ Considering that thermal treatment leads to a significant decrease in pore volume, the H phase is also the most mechanically stable polymorph. On the other side, it presents the lowest acidity due to removal of Brønsted and Lewis acid sites through phase transition.

1.7. Studies about the Impact of Polymorphs in the Catalyst Performance. In account of the differing polymorph properties, their activity and suitability have been evaluated for several reactions such as dehydration of sugars (i.e., glucose and furfuryl alcohol),^{35,36} hydrodeoxygenation of vanillin and 1,6-hexanediol^{37,38}, methane oxidation to formaldehyde,³⁹ and esterification of fatty acids.⁴⁰ In these studies, the polymorphs were obtained via thermal treatment at different temperatures of niobic acid (Nb₂O₅·nH₂O),^{35,36,38} commercial Nb₂O₅,³⁹ and hydrothermally synthesized Nb₂O₅.³⁷

In the acid catalyzed reactions such as dehydration of sugars, an adequate total acidity seems to improve the catalyst performance. According to Eblagon et al.,³⁵ niobic acid was highly active in fructose dehydration at short reaction times, due to its highest acidity between polymorphs. Nonetheless, it enhanced condensation and polymerization reactions to form humins at long reaction times. They also reported that the thermal treatment of niobic acid at 300 °C slightly reduced the acidity, which led to an acceptable sugar conversion without significant degradation of the main product to polymerized side products. Notwithstanding, a high calcination temperature (550 °C) reduced the acidity to a very low level that restricted the extension of dehydration. Similarly, Jun et al.³⁸ observed that the conversion of 1,6-hexanediol through HDO and the selectivity to oily products was related to acidity of the Pt/Nb₂O₅ polymorph. Since the calcination temperature was directly related to the acidity, the following acidity order was observed: Pt/Nb₂O₅ (350 °C) > (500 °C) > (700 °C). The same order was observed in terms of selectivity to oil products. In this sense, the higher amount of Brønsted acid sites on Pt/Nb₂O₅ (350 °C) favored C–O cleavage instead of C–C cleavage, reducing the amount of gas produced.

Zhang and Li³⁷ observed that the oxygen vacancies also played a decisive role, leading to the highest conversion obtained over Ni/Nb₂O₅-T. The oxygen vacancies were responsible for the adsorption and activation of the aldehyde group and further reduction of dissociation energy of the C–OH bond. Finally, the Nb₂O₅-H had the worst catalytic performance. Besides the acid sites and oxygen vacancies, the degree of distortion on the crystalline structure has been pointed out as the determinant to the catalyst performance. Chan et al.³⁶ investigated the impact of Nb₂O₅ polymorphs on the dehydration (oligomerization) of furfuryl alcohol to dimers and trimers. They reported that a transitional polymorph (T/H) had the highest conversion between the polymorphs, despite its low surface area and acidity. The distorted structures at the phase transition (T/H) were believed to have an effect on the catalyst activity, but the selectivity of this polymorph was low. Furthermore, the niobic acid had the second highest conversion rate due to its high acidity. However, it presented a decreasing selectivity to dimers and trimers over time.

The broad range of properties from Nb₂O₅ reinforces its emerging potential in several fields, including as a catalyst. As seen, the catalyst performance is strongly influenced by the catalyst properties, which varies drastically within Nb₂O₅ polymorphs. Therefore, this study aims to evaluate the potential of Nb₂O₅ and the impact of its different polymorphs on the upgrading of pyrolysis oil, with Pd as the active metal. Aiming to correlate catalyst properties and performance, the catalyst (fresh and spent) and the upgraded products were extensively characterized. In addition, the stability of a chosen spent catalyst was tested again after a regeneration process.

2. MATERIALS AND METHODOLOGY

2.1. Materials. **2.1.1. Feed to Be Upgraded.** In this work, a fast-pyrolysis oil from beech wood (BTG – Enschede, The Netherlands) was used after being separated in two different fractions: light phase (FPO-LP) and heavy phase (FPO-HP). During the storage time, a moderate phase separation of the pyrolysis oil was observed and later it was enhanced through intentional aging at 80 °C for 24 h. The aging resulted in two fractions: one denser and rich in organic compounds (FPO-HP – 13.4 wt % water) and another one lighter and rich in water (FPO-LP – 37.7 wt % water). The upgrading of each phase separately was seen as an opportunity to evaluate and later tune the catalysts' properties more appropriately according to their different compositions. Although the FPO-HP had the highest carbon content, the high water and acid contents of the FPO-LP constitute a challenge to be overcome by the catalyst in terms of leaching and pore sintering. Hence, the FPO-LP was chosen to be upgraded with several catalyst compositions in order to evaluate their activity under these challenging feed properties.

2.1.2. Chemicals for Catalyst Synthesis. Nanostructured Nb₂O₅ was prepared with ammonium niobium oxalate (ANO: NH₄[NbO-(C₂O₄)₂(H₂O)₂].(H₂O)_n, kindly provided by CBMM – Companhia Brasileira de Minas e Mineração, Araxá, Brazil). All other Nb₂O₅ supported catalysts were prepared with niobic acid (HY 340 - Nb₂O₅·H₂O, kindly provided by CBMM – Companhia Brasileira de Minas e Mineração, Araxá, Brazil). Pd(NO₃)₂ (no. 205761 - Sigma-Aldrich, St. Louis, USA) was used as the active metal precursor.

2.2. Catalyst Synthesis. **2.2.1. Support Preparation.** To prepare the different polymorphs, a thermal treatment of niobic acid (Nb₂O₅·H₂O) was performed at 1 bar, 4 h heating time, and a heating ramp of 10 °C at different setpoint temperatures: 380, 500, and 800 °C. Niobic acid without pretreatment was also used.

2.2.2. Nanostructured Nb₂O₅. A nanostructured (NS) support was prepared by hydrothermal synthesis with ANO in a Teflon-lined autoclave. The synthesis method applied in this study followed the approach described by Leal et al.¹⁸ First, ANO (3.26 g) was dissolved in water (40.8 mL), and then mixed with 9.2 mL of H₂O₂ (30% v/v) in a molar ratio of 10:1 H₂O₂/Nb. The solution was poured into the autoclave and heated to 175 °C in a silicon oil bath for 17 h (Figure 2). The solid product was washed with distilled water and centrifuged five times before being calcined at 380 °C for 2 h. Due to the calcination temperature, this support was named in this work as NS-TT.

2.2.3. Wet Impregnation. The several Nb₂O₅ polymorphs and the nanostructured support were further impregnated with aqueous solution of Pd precursor to achieve 1 wt % Pd. Before usage, the catalysts were reduced with H₂/N₂ = 30/70 vol % at 350 °C for 2 h with a heating ramp of 5 °C·min⁻¹. For stability tests, a selected catalyst was regenerated before the second use through calcination and reduction under the same conditions applied in the catalyst synthesis.

2.3. Bio-Oil Hydrotreating via HDO. **2.3.1. Batch Setup Description.** An in-house built autoclave (Inconel alloy 625; 200 mL; P_{max} – 36 MPa and T_{max} – 400 °C, IKFT – KIT) was used in this study (Figure 3). The setup was equipped with a magnetically coupled gas injection stirrer (80 N·cm of torque, Premex – Lyss, Switzerland) to enable an efficient mass transfer of hydrogen to the



Figure 2. Setup for hydrothermal synthesis of nanostructured Nb₂O₅ with niobium ammonium oxalate.



Figure 3. Batch reactor for HDO tests.

liquid media, to enhance hydrogenation and, consequently, to prevent polymerization. The autoclave heating was provided by cartridge heaters in a brass jacket, controlled by LabView. A high purity H₂ gas (Air Liquide 6.0, Paris, France) was used for the experiments.

2.3.2. HDO Tests. The HDO was conducted as follows: Before the reaction, the autoclave was charged with 50 g of beech wood pyrolysis oil (FPO-LP) and 2 g of the catalyst to be tested. The batch reactor was then sealed and purged with argon. At room temperature, the setup was pressurized with H₂ until 8 MPa. The reactor was heated to 250 °C with a heating rate of 3.33 °C·min⁻¹. The total reaction time was 2 h, including the heating ramp. After 2 h, the reaction was quenched by cooling with compressed air and then with an ice bath to below 35 °C. The majority of the catalyst tests were performed in triplicate. Additionally, an HDO test of the FPO-LP was performed in the absence of a catalyst.

2.3.3. Product Recovery. After cooling the autoclave, a gas sample was collected. Then, the reactor was completely depressurized before opening. The remaining spent catalysts, solids, and aqueous and oily phases were collected in a centrifuge tube and centrifuged for 30 min at 13,000 rpm (Thermo Scientific Heräus Biofuge Stratos, fixed angle rotor 26 no.75003014, Thermo Scientific, Waltham, USA). The total recovered products consisting of the aqueous phase, upgraded oil, and the recovered solids (spent catalyst + coking products) were weighed before separation. The aqueous and oily phases were then separated and stored. The aqueous phase yield ($Y_{Aq.Phase}$) and the recovered

solid yield ($Y_{Rec.Sol.}$) were directly measured, while the oil phase yield ($Y_{Oil.Phase}$) was calculated as follows:

$$Y_{Oil.Phase} = Y_{total} - Y_{Aq.Phase} - Y_{Rec.Sol.} \quad (1)$$

where Y_{total} is the total yield of the three phases (aqueous, oil, and solid).

2.4. Characterization Methods. **2.4.1. Characterization of Fresh and Spent Catalysts.** The catalysts before and after the HDO reaction were characterized by several techniques. The metal bulk content was analyzed by inductively coupled plasma optical emission spectroscopy (ICP-OES) on an ICP-OES spectrometer Agilent 725 (Agilent, St. Clara, USA). The elemental distribution on the catalyst surface and the catalyst morphology were determined via energy-dispersive X-ray spectroscopy (EDS) and scanning electron microscopy (SEM). SEM was performed on a field emission-SEM DSM 982 Gemini (Carl Zeiss Ltd., Oberkochen, Germany). The surface elemental mapping was performed with a Si(Li) X-ray detector (Inca Pent FET, 30mm² crystal size, Oxford Instrument, Abingdon, UK) coupled to the SEM equipment. The carbon content on spent catalysts was determined via elemental analysis performed on True Spec Macro (LECO Europe). The surface area of the catalysts (BET) was determined via N₂-Physisorption at 77 K on a Belsorp Mini II (Bel Japan Inc., Japan). The crystalline structure of catalysts was evaluated by XRD on X'Pert PRO MPD instrument (PANalytical GmbH, Herrenberg, Germany) endowed with a copper anode (Cu K α 1.54060 Angstrom). The acidity of the catalysts before its use in the HDO was performed at Ruhr University Bochum via ammonia temperature-programed desorption (NH₃-TPD) on a Belcat II (Bel Japan, Japan), coupled with a quadrupole mass spectrometer (MS) ThermoStar (Pfeiffer GmbH, Asslar, Germany).

2.4.2. Characterization of Gaseous Products and H₂ Consumption. The gas sample taken right after reaction quenching was analyzed by gas chromatography. A gas chromatograph 6890 Agilent (Agilent, St. Clara, USA) was used, which was equipped with the valve switching system, two columns, Restek 57096 Hayesep Q and Restek Molsieve 5A, and two detectors, thermal conductivity detector and flame ionization detector (FID). The sample (100 μ L) was injected into the gas chromatograph at an injector temperature of 250 °C. Helium was used as a carrier gas. The oven was initially set at 60 °C for 2 min, heated later to 160 °C at 5 °C·min⁻¹, and finally brought to 250 °C at 15 °C·min⁻¹. The total number of moles in the gas phase inside the reactor was calculated through ideal gas law with measured pressure and temperature before and after the reaction. With these values and the concentration of generated gases and H₂ given by GC, the H₂ consumption as well as the amount of generated gases was calculated.

2.4.3. Characterization of Upgraded Products. The techniques applied in the characterization of the aqueous and oil phases are presented here. The water content was measured by Karl Fischer Titration on a Titrando 841 system (Metrohm, Herisau, Switzerland). Carbon, hydrogen, and nitrogen contents were determined by elemental analysis performed on a Vario EL-cube micro-elemental analyzer (Elementar Analysensystem GmbH, Langenselbold, Germany). The oxygen content was determined by the difference considering the samples were composed only of carbon, nitrogen, hydrogen, and oxygen.

The higher heating value was calculated with the values obtained from elemental analysis, using the following equation,⁴¹ in which the concentration of each element is given in wt %.

$$\begin{aligned} \text{HHV (MJ kg}^{-1}\text{)} = & 0.3491 \cdot \text{C} + 1.1783 \cdot \text{H} - 0.1034 \cdot \text{O} \\ & - 0.0151 \cdot \text{N} + 0.1005 \cdot \text{S} - 0.0211 \cdot \text{ash} \quad (2) \end{aligned}$$

The molecular weight of upgraded products and feedstock was analyzed via gel permeation chromatography (GPC). The measurements were performed on a Merck-Hitachi GPC system, including a L2130 HPLC pump, L2200 autosampler, L2455 DAD-detector, a Guard (50 \times 6 mm) precolumn, and a Viscotec Malvern A2500 (300 \times 8 mm) column. As a result, the number average molecular weight (M_n), the weight average molecular weight (M_w), and the

polydispersity (d) are obtained, which are defined as follows with M_i as the molecular weight of a compound and N_i as the number of compounds:

$$M_n = \frac{\sum (N_i \cdot M_i)}{\sum N_i} \quad (3)$$

$$M_w = \frac{\sum [N_i \cdot (M_i^2)]}{\sum (N_i \cdot M_i)} \quad (4)$$

$$d = \frac{M_w}{M_n} \quad (5)$$

The coking tendency of the feed as well as of the upgraded oils was analyzed via Conradson carbon residue (CCR). The measurements were performed by Grace GmbH (Worms, Germany) on a Alcor MCRT-160 according to ASTM D4530. The upgraded oils, aqueous phases, and both feedstocks were characterized in terms of organic functional groups via proton magnetic resonance ($^1\text{H-NMR}$). The $^1\text{H-NMR}$ measurements were performed at 399.91 MHz on a Varian Inova Unity 400 spectrometer (Varian, Palo Alto, USA) equipped with a 9.4 T Oxford magnet and a 5 mm broadband direct detection probe head (^1H , $X^1\text{H}$, X : heteronucleus 40–162 MHz). The chemical composition was evaluated via gas chromatography (GC–MS/FID). The gas chromatography GC–MS/FID measurements were performed at the Thünen Institute (Hamburg, Germany). Finally, the metal content on upgraded products, possibly leached from the catalyst, was evaluated via ICP-OES, similarly to the measurement of the spent catalysts.

3. RESULTS AND DISCUSSION

3.1. Catalyst Synthesis. Four different Nb_2O_5 supports were obtained through thermal treatment of niobic acid ($\text{Nb}_2\text{O}_5 \cdot n\text{H}_2\text{O}$) at four conditions (Table 1). Additionally, a

Table 1. Catalyst Preparation Conditions and Correspondent Names Based on the Polymorphs Identified via X-ray Diffraction

starting material	thermal treatment before Pd impregnation	calcination after Pd impregnation/reduction	code
niobic acid ($\text{Nb}_2\text{O}_5 \cdot n\text{H}_2\text{O}$)	not treated	380 °C/350 °C	Pd/A- Nb_2O_5
	380 °C		Pd/TT&A- Nb_2O_5
	500 °C		Pd/T&TT- Nb_2O_5
	800 °C		Pd/M&T- Nb_2O_5
NS- Nb_2O_5 (hydrothermal synthesis)	380 °C	380 °C/350 °C	Pd/NS-TT- Nb_2O_5

fifth Nb_2O_5 support was hydrothermally synthesized with niobium oxalate. These five supports were impregnated with Pd as an active metal precursor (Pd – 1 wt %), calcined again and reduced before the tests. For simplicity, the 1 wt % was omitted when naming catalysts.

The synthesized catalysts were named according to the polymorphs detected or expected at each thermal treatment temperature, and the catalyst prepared through hydrothermal synthesis was also referred as NS, due to its nanostructured surface. In the text, the term niobic acid always refers to the commercial compound $\text{Nb}_2\text{O}_5 \cdot n\text{H}_2\text{O}$ used as the starting material to prepare most of the catalysts, except the hydrothermally synthesized catalyst.

In this work, the catalysts were characterized in terms of crystalline structure, surface area, morphology, metal loading and acidity. Later, the performance of the catalysts toward the

bio-oil upgrading through HDO was evaluated and correlated with their described properties.

3.2. Catalyst Characterization. **3.2.1. Crystalline Structures.** The thermal treatment of niobic acid ($\text{Nb}_2\text{O}_5 \cdot n\text{H}_2\text{O}$) at different temperatures leads to several polymorphs with different crystalline structures that can be accessed over X-ray diffraction. In the literature, the topic of crystalline structures of Nb_2O_5 polymorphs is surrounded by a long and ongoing discussion. The unit cell of some polymorphs has been long elucidated, while some are still under intense debate.³² Moreover, due to the large number of Nb_2O_5 phases described in the literature and the absence of a cohesive nomenclature system, the assignment of the observed diffraction patterns and the respective reference polymorph revealed to be rather than challenging. Considering that, the observed patterns were attributed to one or more reference patterns based on several studies.^{21,24,33,42}

The diffraction patterns of the catalysts as well as the assigned reference patterns are shown in Figure 4. As expected, the calcination temperatures strongly affected the crystalline structures of Nb_2O_5 and, consequently, the diffraction patterns. Niobic acid, used as the starting material for most of the supports, had no diffraction peaks due to its amorphous nature. Remarkably, Pd/A- Nb_2O_5 prepared directly with niobic acid was also amorphous, despite the calcination of the Pd precursor (350 °C) and reduction at 350 °C.

The broad peaks observed in the diffractogram of Pd/TT&A- Nb_2O_5 prepared with niobic acid thermally treated at 380 °C pointed out to an initiated poor crystallization. The large peaks may be related to TT- Nb_2O_5 polymorph (ICCD 00-007-0061, ref 28). Despite the same calcination temperature applied on Pd/TT&A- Nb_2O_5 , these TT- Nb_2O_5 characteristics peaks were more defined on the Pd/NS-TT- Nb_2O_5 . The high surface area of the Pd/NS-TT- Nb_2O_5 prepared via hydrothermal synthesis may have enhanced the crystallization process. This is in agreement with Schäfer et al.,²¹ who reported that the phase transitions of Nb_2O_5 are significantly dependent on the starting materials.

With a further increase in the thermal treatment temperature of niobic acid to 500 °C, the diffraction peaks were more intense and better defined (Pd/T&TT- Nb_2O_5). Two possible polymorphs, the orthorhombic T phase (ICSD no. 1840, ref 33) and the pseudo-hexagonal TT phase (ICCD 00-007-0061, ref 28), could be ascribed to this catalyst. According to Weissman et al.,³⁰ distinguishing between the diffraction patterns from TT and T is rather challenging. In agreement, Ko and Weissman²² stated that the TT and T polymorphs have similar patterns and structures that differ only in subtle ways, which can hinder their discrimination except under ideal circumstances. Ko and Weissman²² also mentioned that the main differences between both polymorphs are that some oxygen atoms from the T phase are replaced by monovalent species such as OH^- , Cl^- , or vacancies on the TT phase. In addition, on the TT phase, Nb atoms are allowed to occupy a range of positions between two equivalent sites, while on the T polymorph Nb atoms are restricted to either one or the other of these similar sites. Thus, the TT diffractogram presents broad peaks and no peak splitting like the T pattern. With this in mind, it was not possible to exclusively define the polymorph present in the Pd/T&TT- Nb_2O_5 , regardless of an intense effort.

A mixture of polymorphs was obtained through the calcination of niobic acid at 800 °C. Patterns attributed to T

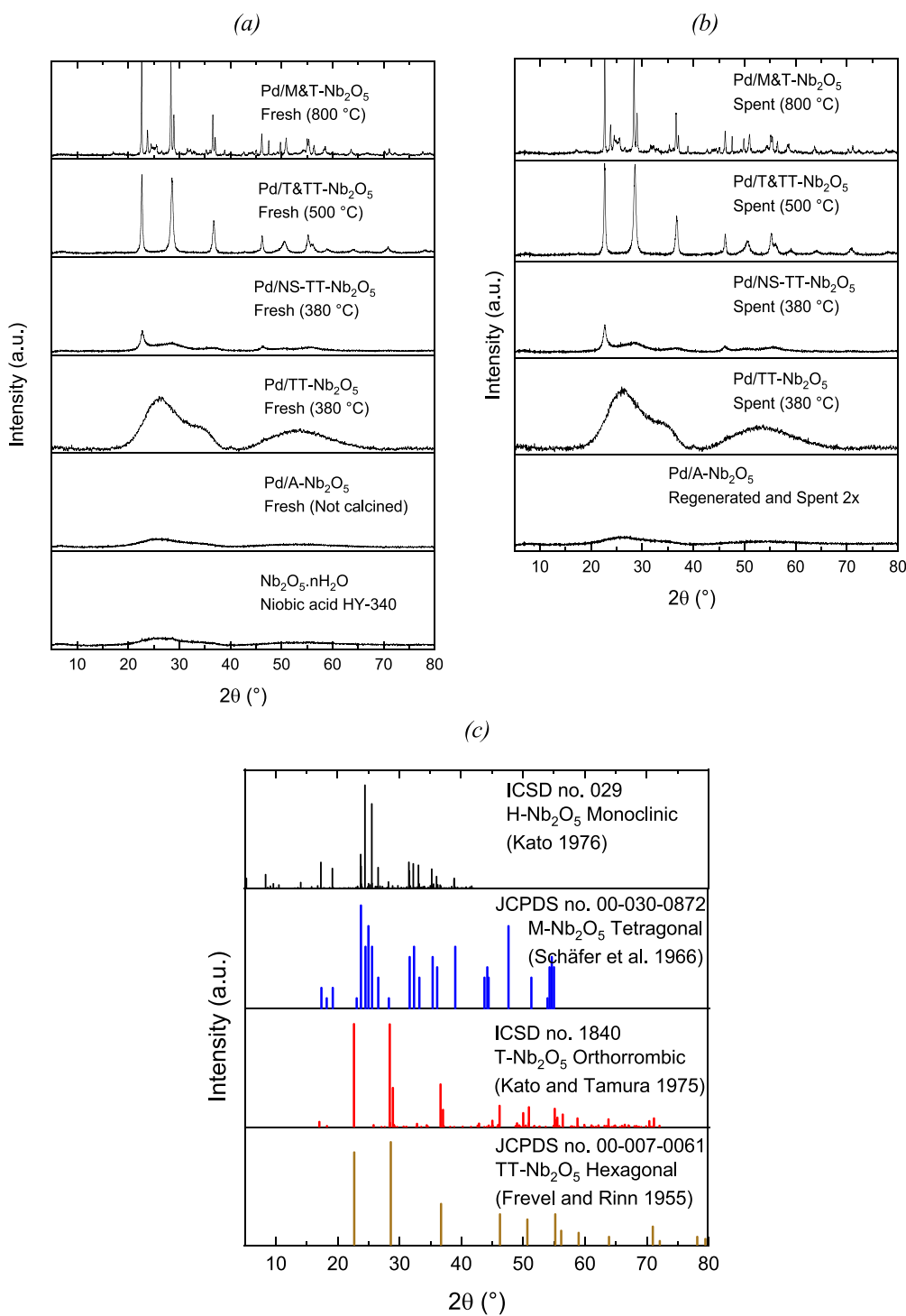


Figure 4. XRD diffractogram of fresh catalysts (a), of spent catalysts (b), and reference patterns of Nb₂O₅ polymorphs (c).

phase (ICSD no. 1840, ref 33) were detected, including several characteristic doublets (22.6, 28.3, 28.9, 36.5, 37.0, 46.2, 49.8, 51.0, 55.0, and 55.3 $^\circ$). Additionally, patterns from the tetragonal M phase (ICCD 00-030-0872, ref 21) were also identified (23.7, 24.4, 24.9, 25.5, 31.5, 32.3, 35.3, 38.9, and 47.5 $^\circ$). The M phase is reported in the literature as a metastable phase present in the transition between T and H polymorphs. Moreover, the H monoclinic polymorph (ICSD no. 29, ref 34) is also possibly present in the mixture considering all the similarities on the H and M reference patterns.

The diffraction patterns of all fresh catalysts are similar to their corresponding spent catalyst patterns, confirming that the crystalline structure remained unchanged through HDO and through regeneration. Finally, related to the active metal, no signals ascribable to Pd were detected in the above-mentioned patterns.

3.2.2. Catalyst Surface Areas, Morphology, and Active Metal Content on the Surface. The SEM-EDS pictures of different supports as well as synthesized catalysts are shown in Figure 5. The catalysts surface areas measured via BET with N₂ desorption are placed in Table 2. The hydrothermally

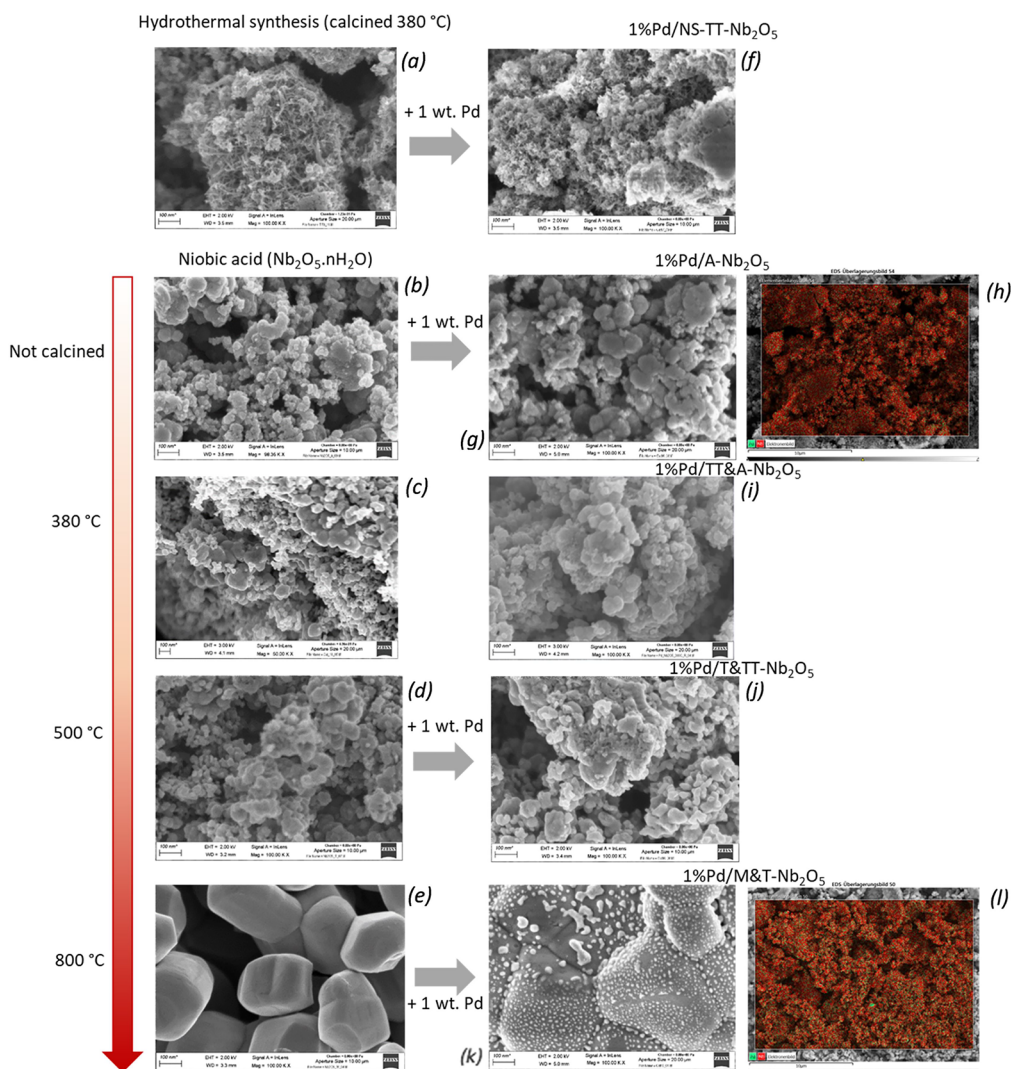


Figure 5. Morphology and active metal distribution of hydrothermally synthesized Nb_2O_5 (a), niobic acid as received (b) as well as calcined at 380 °C (c), 500 °C (d), 800 °C (e), and impregnated catalysts: Pd/NS-TT- Nb_2O_5 (f), Pd/A- Nb_2O_5 (g, h), Pd/T&TT- Nb_2O_5 (i), Pd/TT&A- Nb_2O_5 (j), Pd/M&T- Nb_2O_5 (k, l). Pd is displayed in green, and the Nb_2O_5 support is red.

Table 2. Fresh or Freshly Regenerated Catalyst Properties: Surface Area, Metal Content on the Surface and Acidity

fresh catalyst	thermal treatment ^a	surface area	Pd (EDS ^b wt %)	desorbed NH_3 (mol g ⁻¹)	peak NH_3 -TPD (°C)
Pd/TT-NS- Nb_2O_5	HS-380 °C	167.0	1.16	7.1×10^{-4}	244
Pd/A- Nb_2O_5		102.1	1.81	2.2×10^{-4}	213
Pd/TT&A- Nb_2O_5	380 °C	<i>n.m.</i>	1.34	3.1×10^{-4}	226
Pd/T&TT- Nb_2O_5	500 °C	38.7	0.98	4.3×10^{-5}	209
Pd/M&T- Nb_2O_5	800 °C	1.6	1.93	0	
Pd/ Nb_2O_5 -A reg.		78.0	<i>n.m.</i>	3.8×10^{-4}	216

^aThermal treatment of the support before impregnation. ^bEDS performed with fresh catalysts. HS: hydrothermal synthesis. *n.m.*: not measured.

synthesized Nb_2O_5 (NS- Nb_2O_5) had a nanostructured surface visible through SEM as thin fibers (nanorods – Figure 5a). The nanostructured catalyst had the highest surface areas between the catalysts (Pd/NS-TT- Nb_2O_5 –167.0 m² g⁻¹).

The niobic acid thermal treatment before impregnation promoted pore sintering that was proportional to the setpoint temperature (Figure 5b–e). This reflected on the reduction of catalyst surface area prepared with calcined supports, also depending on the temperature (Table 2). Hence, the catalyst prepared with niobic acid calcined at 800 °C had a highly sintered surface, without pores and with a flat topography. The

extremely small and unbranched surface of this support resulted on a peculiar and intense agglomeration of Pd despite of its small loading (1 wt %). In contrast, the not calcined niobic acid and the niobic acid calcined at 380 °C had much smaller grains, irregular topography and a high porosity. Similarly, the heat of the calcination and reduction processes applied to regenerate of the catalyst Pd/A- Nb_2O_5 reduced its surface area.

The metal content on the fresh catalyst surface was determined via EDS (Table 2). As expected due to the wet impregnation method, the metal concentration on the catalyst

surface was higher than the nominal values, the latter being calculated according to the total catalyst weight.

3.2.3. Catalyst Surface Acidity. The acidity of the catalysts was evaluated through ammonia temperature-programmed desorption (TPD-NH₃) (Table 2). As discussed later in Section 3.2, the acid sites had a crucial impact on the catalyst activity. Especially the oxophilic sites represented by the Nb⁴⁺/Nb⁵⁺ cation are quoted as crucial in the absorption of oxygenated species and thus important for the HDO. On the other side, strong acid sites led to strong adsorption, which can result in the accumulation of intermediates and further catalyst deactivation through coke formation.

Based on the amount of ammonia adsorbed on the catalyst surfaces, the thermal treatment of niobic acid reduced its acidity proportionally to the temperature. Thus, the highest calcination temperature (800 °C) led to a neutral catalyst.

Remarkably, the highest acidity was observed on the hydrothermally synthesized catalyst (Pd/NS-TT-Nb₂O₅) despite the same calcination temperature applied as on Pd/TT&A-Nb₂O₅. In agreement with the literature, the hydrothermal synthesis contributes not only to the high surface area but also to the high acidity.

While heating at 800 °C destroyed all acid sites, the thermal treatment of niobic acid at low temperatures (380 °C) actually slightly increased the catalyst acidity. In a similar way, the regeneration of the spent catalyst (Pd/A-Nb₂O₅) at 350 °C slightly increased its acidity. Tanabe²⁵ observed that the thermal treatment of Nb₂O₅·*n*H₂O at circa 300 °C increased the amount of Lewis acid sites, but it decreased at higher thermal treatment temperatures. Nonetheless, he also stated that in contrast to Lewis acid sites, the amount of Brønsted acid sites decreases due to dehydration and phase transition processes.

3.2.4. Coking and Reusability of Catalysts. The spent catalysts were evaluated in terms of the active metal content (ICP-OES), carbon content, and crystalline structure. The results are provided in Table 3. The bulk metal contents of the catalysts after the HDO were close to nominal values, indicating that the leaching of active metal was negligible.

Table 3. Spent Catalyst Properties: Metal Content on the Surface and Carbon Content^a

spent catalyst	Pd (ICP-OES ² wt %)	C (wt %)
Pd/TT-NS-Nb ₂ O ₅	0.88	8.9
Pd/A-Nb ₂ O ₅	1.04	6.0
Pd/TT&A-Nb ₂ O ₅	0.78	<i>n.m.</i>
Pd/T&TT-Nb ₂ O ₅	0.89	2.6
Pd/M&T-Nb ₂ O ₅	0.82	4.2
Pd/Nb ₂ O ₅ -A reg.	0.72	5.5

^a*n.m.*: not measured.

The carbon content on spent catalysts was evaluated as an indicator of the coke formation during the HDO. The observed tendency was that the higher the catalyst acidity, the higher the coking formation. Therefore, the most acid catalyst (Pd/NS-TT-Nb₂O₅) led to the highest carbon content (8.9 wt %), which may be related to the accumulation of oxygenated compounds adsorbed on acid sites. The exception was the Pd/M&T-Nb₂O₅, the least acidic catalyst but with a moderate coking formation (4.2 wt %), probably related to the high polymerization observed in this test. The spent

regenerated catalyst (Pd/Nb₂O₅-A reg.) led to a similar coke formation to the fresh catalyst (Pd/A-Nb₂O₅).

3.3. Catalysts Tests with Bio-Oil. The synthesized and characterized catalysts were tested in terms of activity and products composition using the light phase of beech wood oil (FPO-LP). To enable the evaluation of catalysts in such a complex feed, several complementary techniques were applied, and the results are discussed as follows.

3.3.1. H₂ Consumption and Catalyst Activity. Considering the complexity of the feed FPO-LP, the H₂ uptake is an important indicator of the catalyst activity during the upgrading. Several hydrogen-involving reactions may take place within the HDO such as hydrogenation, hydrogenolysis, and hydrocracking. In Figure 6, the H₂ consumption during the upgrading process over each catalyst is shown.

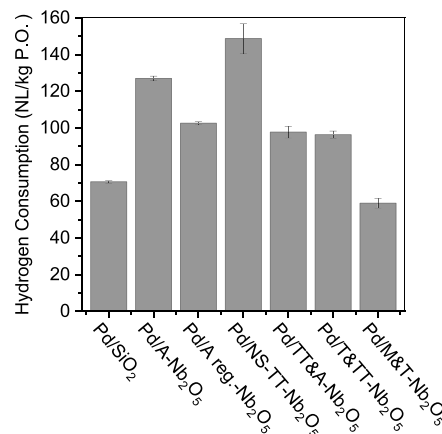


Figure 6. H₂ consumption in NL/kg P.O. during the HDO of FPO-LP with Pd catalysts supported on several Nb₂O₅ polymorphs. While all other catalysts were fresh, the Pd/A-reg. Nb₂O₅ was used after regeneration. Data from Pd/SiO₂ were taken from Campos Fraga et al.¹⁹

Pd catalysts supported on Nb₂O₅ presented significantly higher H₂ consumption (58.9–148.8 NL/kg_{P₂O}) than Pd/SiO₂ (70.4 NL/kg_{P₂O}). Different from SiO₂, Nb₂O₅ can promote H₂ spillover, which consists of the migration of activated hydrogen atoms from metal sites to the vicinity of oxygen vacancies, improving the dispersion of hydrogen in the catalyst surface.⁴³ Analogous to a higher catalyst surface area with better-dispersed metal sites, it enhances hydrogen-involving reactions as hydrogenation and hydrogenolysis as shown in Sections 3.3.4 and 3.3.6.

Between Nb₂O₅ polymorphs, the nanostructured one (NS-TT-Nb₂O₅) had the highest H₂ uptake and consequently the highest hydrogenation and hydrogenolysis activities due to the (i) high catalyst surface area, and consequently improved Pd dispersion, but also due to the (ii) high acidity dispersed in the larger area. The acid sites, especially the oxophilic sites (Nb⁴⁺/Nb⁵⁺), are essential for the adsorption of oxygenated compounds and consequently further reactions such as hydrogenation and hydrogenolysis.⁴⁴ The beneficial impact of acid sites explained the decrease of H₂ uptake with the increase in the thermal treatment temperature and consequent decrease in acidity (Table 2). Thus, the lowest H₂ consumption over the neutral Pd/M&T-Nb₂O₅, and consequent limited hydrogenolysis and hydrogenation activity (Section 3.2.4).

Nonetheless, Mendes et al.⁴⁴ also stated that although the acid sites are crucial for successful HDO, they could also catalyze coke formation. The favored adsorption of oxygenated sites on acid sites without further reaction such as hydrogenation and hydrogenolysis could result in the accumulation of intermediates and subsequent polymerization and coking. According to them, an optimal value of acidity is required. In our view, this value is definitely dependent on the surface area. Nonetheless, it is important to emphasize that although Pd/TT&A-Nb₂O₅ had higher acidity than Pd/A-Nb₂O₅, the reduction of surface area may be the reason for the lower H₂ uptake of Pd/TT&A-Nb₂O₅. Similarly, the regeneration of Pd/A-Nb₂O₅ led to reduction on the H₂ uptake during the second HDO. In this case, as detailed in Table 2, although the acidity slightly increased compared to the fresh catalyst, the surface area suffered a significant reduction. Hence, the sintering effect was more relevant than the acidity.

3.3.2. HDO Product Yields and Composition of Gaseous Products. In Figure 7, the product distribution after HDO is

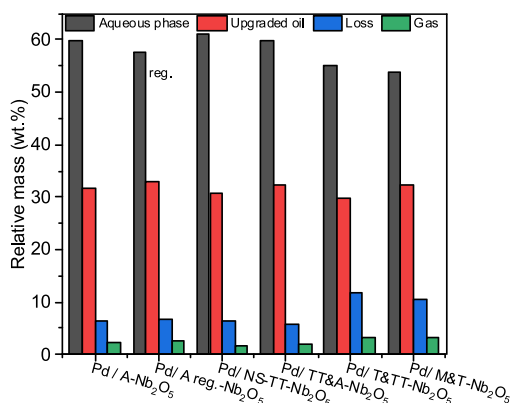


Figure 7. Product distribution after HDO on Pd/Nb-based catalysts.

presented for all catalysts. The HDO products were mainly divided into three phases: aqueous phase (60.3–65.4 wt %), upgraded oil (32.7–36.3 wt %), and gas phase (0.9–1.7 wt %). Product losses (3.0–5.3 wt %) were unavoidable and mainly caused by the remaining upgraded oil on the reactor walls and stirrer.

Because of the high water content in the feed FPO-LP (37.7 wt %) and the formation of water during HDO, the aqueous phase corresponded to more than 60 wt % of the products. The Nb₂O₅ polymorphs had a significant impact on the aqueous phase yields. In terms of aqueous phase amount obtained with different polymorphs, the following order was observed: Pd/M&T-Nb₂O₅ < Pd/T&TT-Nb₂O₅ < Pd/A-Nb₂O₅ = Pd/TT&A-Nb₂O₅ < Pd/TT-NS-Nb₂O₅. This tendency was related to the amount of water produced during HDO, referred here as hydrogenolysis. Furthermore, the polarity of the compounds also influenced on the partition of phases.

In turn, the upgraded oil yield was influenced by the losses of products but also by the aqueous phase yield. The migration of water and small oxygenated organic molecules to the aqueous phase intrinsically reduced the weight of the remaining oily phase. Hence, an opposite trend from the aqueous phase yield was observed on the upgraded oil yield.

The composition and quantification of the generated gases during HDO are presented in Figure 8. The amount of generated gases over the polymorphs followed the order: Pd/

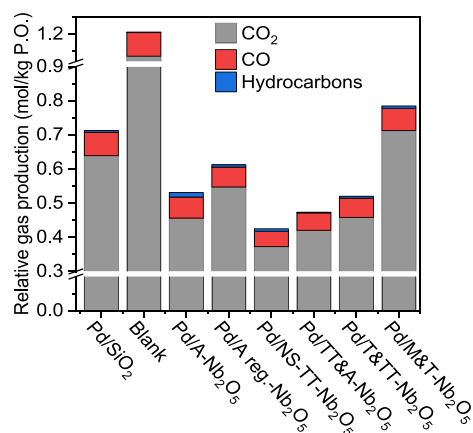


Figure 8. Generated gases during HDO for the different catalysts and in the absence of a catalyst. Data from Pd/SiO₂ were taken from Campos Fraga et al.¹⁹

TT-NS-Nb₂O₅ < Pd/TT&A-Nb₂O₅ < Pd/T&TT-Nb₂O₅ < Pd/A-Nb₂O₅ < Pd/M&T-Nb₂O₅. This is mostly the opposite trend as the amount of water produced, and both were an indicator of the catalysts activity as discussed later. CO₂ was the main gas generated over the catalysts and, in general, CO₂ production decreased with the H₂ uptake (Section 3.3.1). The Pd/M&T-Nb₂O₅ had the highest CO₂ production between catalysts, the lowest H₂ uptake and strongly polymerized oils. This was related to the absence of acid sites, a sintered surface (Table 2), and a low Pd dispersion (Figure 5). In turn, Pd/NS-TT-Nb₂O₅ had the lowest CO₂ production and the highest H₂ consumption, in agreement with the highest surface area and consequently good Pd dispersion, as well as the highest acidity (Table 2).

CO₂ production was also related to the polymerization degree with the upgraded oils. In agreement with that, De Miguel Mercader et al.¹⁴ reported that, in their experiments, the extension of CO₂ production was related to the extension of polymerization reactions. Furthermore, they pointed out to an existing competition between polymerization and hydro-treating reactions.

An exception to this H₂ uptake vs CO₂ generation trend was the catalysts Pd/A-Nb₂O₅. It had a CO₂ production higher than Pd/TT&A-Nb₂O₅ and similar to Pd/T&TT-Nb₂O₅ despite its H₂ uptake higher than those two catalysts. This may be related to H₂ being used more for hydrogenolysis than for hydrogenation. Nonetheless, further investigations are required to better understand this behavior.

The second main gas was CO with small variation between the catalysts. Besides CO and CO₂, saturated and unsaturated hydrocarbons (C₂–C₄) were also produced in small amounts during HDO, and the detailed composition of these gaseous hydrocarbons is provided in the Supplementary Material (Figure S1).

3.3.3. Bio-Oil Polymerization during HDO. The polymerization extension of upgraded oils was verified through visual analysis (Figure 9) and through gel permeation chromatography for selected catalysts (Figure 10). Previously published results for Pd/SiO₂¹⁹ are shown here for comparison. It is important to highlight that the GPC device was not calibrated with standards and, therefore, the values shown in Figure 9 are relative molecular weight values. This way, these values cannot be compared with other literature results, but they are useful for comparison of the different oils within this work.

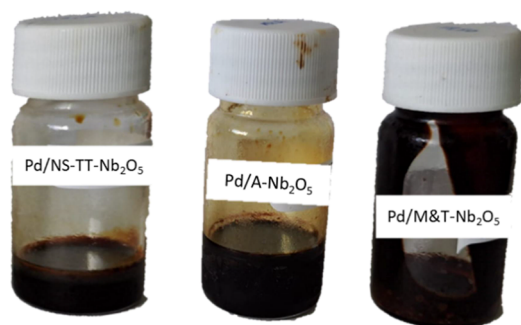


Figure 9. Polymerized upgraded oil obtained over Pd/M&T-Nb₂O₅ in comparison with a nonpolymerized upgraded oil obtained over Pd/A-Nb₂O₅ and over the nanostructured catalyst Pd/NS-TT-Nb₂O₅.

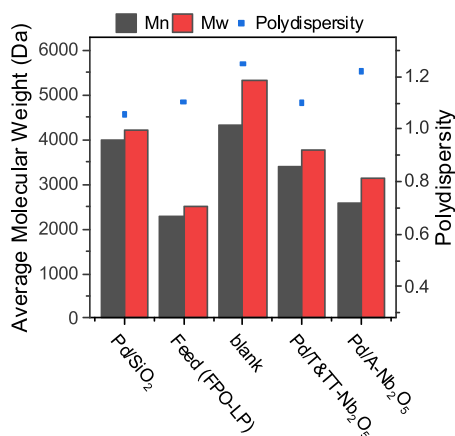


Figure 10. Number average molecular weight (M_n), weight average molecular weight (M_w) and polydispersity of feed (FPO-LP), and upgraded oils obtained through HDO over selected catalysts. Data from Pd/SiO₂ were taken from Campos Fraga et al.¹⁹

The broad range of different oxygenated organic groups inside bio-oil makes it prone to polymerization reactions under thermal treatment. Thus, polymerization is a big issue for the HDO of bio-oil and the main reason for coke formation.⁴⁵ The dependence of the polymerization extension of the catalyst activity was clearly visible through blank experiment. Although it resulted in a decrease of oxygen, this decrease happened at the expenses of a stone-like char product.¹⁹ When using low-activity catalysts, the enhanced polymerized product tends to accumulate on the catalyst surface and further reduce its activity, in a cascade effect. Cordero-Lanzac et al.⁴⁶ proposed two main pathways for polymerization and consequent catalyst deactivation. The first pathway was described as a recombination of oxygenated compounds such as alkyl phenols and acetic acid, while the second was related to the formation of polyaromatic structures through condensation of alkyl aromatics.

In contrast, over active catalysts, reactive oxygenated compounds as aldehydes, ketones, and C–C double bonds may be converted to more stable groups instead of undergoing polymerization. Thus, there is a competition between polymerization and hydrotreating reactions, as pointed by De Miguel Mercader et al.¹⁴ The H₂ availability is a determinant factor for the deactivation of reactive compounds through hydrogenation.¹⁴ In the same way, the adsorption and cleavage of H₂ molecules into hydrogen radicals on the metal sites are

essential, thus the better ability of noble metals to prevent polymerization.⁴⁵

In this study, the upgraded oils had higher average molecular weight than the feed (FPO-LP), which could erroneously lead us to an assumption of general polymerization. Instead, this is explained by the preference of large molecules for the organic phase, and the preference of water and other small polar compounds for the aqueous phase.

In general, Nb₂O₅-supported catalysts led to smaller average molecular weight than SiO₂, in agreement with their higher H₂ uptake (Section 3.3.1) and consequent deactivation of reactive compounds prone to polymerization. Similarly, the Pd/A-Nb₂O₅ led to an upgraded oil with smaller average molecular weight than Pd/T&TT-Nb₂O₅, also in agreement with the H₂ uptake. The higher acidity of Pd/A-Nb₂O₅ in the presence of suitable hydrogenation sites may have minimized polymerization through adsorbing oxygenated compounds and further deactivating them by hydrogenation. In turn, the neutral and sintered catalyst Pd/M&T-Nb₂O₅ led to the most polymerized oil (Figure 10), also in agreement with its smallest H₂ uptake between Nb₂O₅ catalysts.

3.3.4. Elemental Composition and Water Content on Upgraded Products and Feed. One goal of the HDO is to maximize the transfer of carbon and hydrogen from the feed to the upgraded oil, while minimizing its oxygen content, which should be transferred to the aqueous phase in the form of water. The elemental composition of each upgraded product is dependent on the partition of the molecules between the liquid phases (aqueous and oil) and, consequently, on the polarity of the produced compounds and the water content.

In Table 4, the elemental composition and the HHV of the feed and the HDO products are presented. As aimed, the water originally from the feed (circa 37.7 wt % of FPO-LP) plus the generated water during HDO was concentrated in the aqueous phase (water content: 67.3–72.8 wt %). In turn, the upgraded oil had circa 7-fold less water content (6.8–10.2 wt %). Consequently, the carbon from the feed FPO-LP (32.9 wt %, wet basis) was mostly concentrated on the upgraded oil (carbon content between 60.0 and 64.9 wt %). In contrast, the aqueous phase had a low carbon content (13.7–17.0 wt %). Most of the organic oxygen content was concentrated in the aqueous phase (31.4–35.3 wt %), due to the preferential accumulation of small polar oxygenated organic compounds in this phase. Finally, the organic oxygen content decreased from 40.7 (FPO-LP) to 23.7–28.0 wt % in the upgraded oils. Consequently, the HHV of the upgraded oil increased significantly (25–44%).

The polarity of the compounds and the final water content are both affected by the catalyst activity. Since the polarity of the compounds is influenced by the molecular weight and thus by the polymerization degree, polymerized upgraded oils as the one obtained over Pd/M&T-Nb₂O₅ and the blank test had much lower water content and higher carbon content. The similar behavior was observed by Miguel de Mercader¹³ about the high-pressure thermal treatment (HPTT) of pyrolysis oil. Nonetheless, as he pointed out, these apparent improvements happened at the expenses of high coking tendency, which made the coprocessing of HPTT oil in an FCC unit with long residue fossil feed unfeasible. In this sense, the polymerization degree should always be analyzed together with the elemental composition.

Besides the absolute values, the O/C and H/C ratios of upgraded oils presented in the Van Krevelen diagram were

Table 4. Elemental Composition and HHV (MJ kg⁻¹) of FPO-LP, of Upgraded Oils and Aqueous Phases Obtained by HDO^a

	feed	blank	Pd/SiO ₂	Pd/A-Nb ₂ O ₅	Pd/A reg. Nb ₂ O ₅	Pd/NS-TT-Nb ₂ O ₅	Pd/TT&A-Nb ₂ O ₅	Pd/T-Nb ₂ O ₅	Pd/M&T-Nb ₂ O ₅
aqueous phase									
wet basis (wt %)									
C	32.90	12.20	13.90	15.73	15.30	17.00	16.10	16.40	13.70
H	8.10	9.90	9.60	10.03	9.90	10.00	10.90	10.50	9.90
N	0.14	1.70	2.40	2.27	2.20	2.00	1.70	1.70	2.43
H ₂ O	37.70	73.20	71.35	69.00	70.20	67.30	69.40	68.70	72.17
O	58.86		74.10	71.97	72.60	71.00	71.30	71.40	73.97
dry basis (wt %)									
C	52.81		48.52	50.75	51.34	51.99	52.61	52.40	49.23
H	6.28		5.84	7.63	7.05	7.71	10.42	9.16	6.76
N	0.22		8.39	7.31	7.38	6.12	5.56	5.43	8.75
O	40.69		37.25	34.30	34.23	34.18	31.41	33.01	35.27
HHV	21.6		19.5	23.1	22.6	23.6	27.3	25.6	21.4
upgraded oil									
wet basis (wt %)									
C		62.50	64.15	61.23	63.20	58.6	64.00	60.00	64.90
H		6.30	7.20	6.97	7.20	7.5	7.80	6.40	6.80
N		0.10	0.10	0.13	0.10	0.1	0.20	0.20	0.13
H ₂ O			7.00	9.13	7.90	10.2	8.90	8.80	6.83
O		31.10	28.55	31.67	29.50	33.8	28.00	33.40	28.17
dry basis (wt %)									
C			68.98	67.39	68.62	65.26	70.25	65.79	69.66
H			6.90	6.55	6.86	7.09	7.48	5.95	6.48
N			0.11	0.15	0.11	0.11	0.22	0.22	0.14
O			24.01	25.92	24.41	27.54	22.05	28.05	23.71
HHV			29.7	28.6	29.5	28.3	31.1	27.1	29.5

^aData from Pd/SiO₂ taken from Campos Fraga et al.¹⁹

used to compare different catalysts (Figure 11). Considering the values for crude oil, an O/C close to zero and a moderate

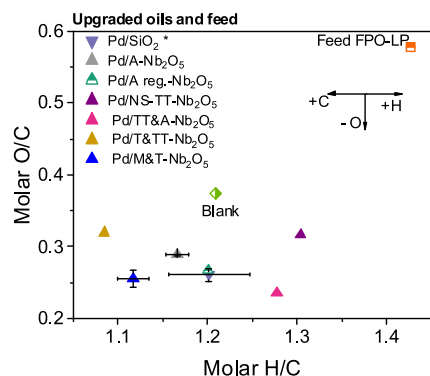


Figure 11. Van Krevelen diagram of feed (FPO-LP) and upgraded oils obtained over Pd catalysts. Data from Pd/SiO₂ were taken from Campos Fraga et al.¹⁹

H/C of around 1.5 are desirable.⁴⁷ Nonetheless, these values should be achieved by decreasing oxygen content and increasing hydrogen, and not by decreasing the carbon content, which would negatively affect the carbon recovery. In agreement with data compiled by Venderbosch et al.,⁴⁷ the H/C of the feed (1.43) decreased on upgraded oils. The smaller H/C ratio of upgraded oil despite of the H₂ insertion had two possibly reasons: (i) the removal of water partially at the expenses of H atoms already in the organic compounds inside the feed, and (ii) the carbon increase due to phase separation from the preferential accumulation of larger organic compounds into the oily phase.

Between the catalysts, the nanostructured catalyst Pd/NS-TT-Nb₂O₅ with the highest surface area and the highest acidity led to the upgraded oil with the highest H/C value (1.31), in agreement with the highest H₂ uptake. Following, the Pd/TT&A-Nb₂O₅ had the second highest H/C value, in agreement with the second highest catalyst acidity. Although Pd/A-Nb₂O₅ had a higher H₂ uptake than Pd/TT&A-Nb₂O₅, more H₂ was consumed for water formation than for hydrogenation, explaining the lower H/C of the former. The Pd/M&T-Nb₂O₅ had one of the lowest H/C ratio (1.12), due to its sintered and neutral surface. The regeneration slightly increased H/C over Pd/A-Nb₂O₅, possibly related to the slight increase of acidity.

The O/C ratio of feed FPO-LP decreased from 0.58 to 0.24–0.32 in the upgraded oils obtained over Nb₂O₅ catalysts, due to the removal of oxygen and the increase of carbon content. Between the catalysts, the variation on O/C ratios was not significant, in contrast to the H/C values. The smaller O/C was obtained over Pd/TT&A-Nb₂O₅ followed by Pd/M&T-Nb₂O₅ and Pd/SiO₂. In the case of Pd/M&T-Nb₂O₅ and Pd/SiO₂, the lower O/C ratios happened at the expenses of polymerization. This was associated to high CO₂ and CO generation and long organic chains, which increased carbon content and repealed oxygenated organic molecules to the aqueous phase. Nonetheless, similar to HPTT oils, highly polymerized oils may not be appropriate for co-feeding.¹³

3.3.5. Coking Tendency of Upgraded Oils. According to Talmadge et al.,⁴⁸ the tendency of the hydrocarbon stream to form carbon deposits at elevated temperatures is an important specification considered on crude oils, which is relevant to take into account, if co-feeding of bio-oil is aimed. Bio-oil has a natural tendency to form carbonaceous residues when heated,

and this can be measured for example through the Conradson Carbon Residue test (CCR). The absolute values of CCR of selected upgraded oils and feed are presented in Table 5, as

Table 5. Micro Conradson Carbon Residue (CCR) of Feed FPO-LP and Upgraded Oils Obtained over Several Catalysts^a

catalyst	Micro Conradson carbon residue (wt %)	carbon residue/total carbon content (wt %)
FPO-LP	13.0	39.5
Pd/A-Nb ₂ O ₅	16.1	26.3
Pd/TT-NS-Nb ₂ O ₅	12.4	20.6
Pd/TT&A-Nb ₂ O ₅	18.0	29.5
Pd/T&TT-Nb ₂ O ₅	20.2	33.7

^aThe normalized CCR values considering the total carbon content.

well as the normalized values considering the total carbon content. The feed and upgraded oils had fold higher CCR values than typical crude oil values (1.7 wt %, ref 49), but also higher than some values reported in the literature for catalytic hydrotreated oils.⁵⁰ While these oils reported in the literature were deeply deoxygenated, which explains the lower CCR values, the strategy in the present work was to promote a mild hydrodeoxygenation, also called stabilization.

Most upgraded oils had higher CCR values than the feedstock, likewise the molecular weight. Possibly, the increase in the carbon residue is rather related to the accumulation of larger compounds in the upgraded oil, considering the higher hydrogen content during HDO. Therefore, the normalized values are a better description of the carbon fraction that tends to remain as coke. The smaller coking tendency was achieved over the nanostructured catalysts (Pd/NS-TT-Nb₂O₅), in agreement with their highest hydrogenation activity. In addition, increasing the intensity of the support thermal treatment led to an increase in carbon residue. Again, this is in agreement with the decrease in the hydrogenation activity, related to the reduction of acidity and surface area.

3.3.6. Hydrogenolysis – Water Formation during HDO. The formation of water during HDO is one of the main pathways for H₂ consumption. Although the water contents in each product phase are discussed in Section 3.3.5, in order to access the hydrogenolysis activity of the catalysts, the calculation of the total amount of water generated during HDO is essential. Hence, the formation of water was calculated considering the theoretical mass balances and the water content in both upgraded products (aqueous phase and upgraded oil), excluding the amount of water already present in the feed (FPO-LP).

The amount of water generated during HDO over the catalysts is shown in Figure 12. The Nb₂O₅-supported catalysts had significantly higher hydrogenolysis than the SiO₂ catalyst.¹⁹ This is based on the unique promotion effect of C–O bond cleavage from Nb₂O₅, and this ability is explained by some of its properties as the oxophilic sites.⁵¹ The oxophilic sites of Nb₂O₅, especially Nb⁴⁺ and Nb⁵⁺, are accounted to promote a good adsorption between the oxygen in biomass-derived molecules (e.g. lignin), which reduces the dissociation energy of C–O bonds, facilitating their cleavage.^{52,53}

Another Nb₂O₅ property pointed as key for the enhanced hydrogenolysis was the surface acidity.⁵¹ Herein, the influence of the acidity on the water formation was clear when comparing Nb₂O₅ with SiO₂, but also between the Pd catalysts

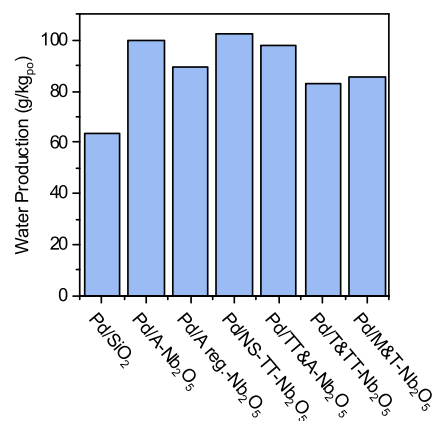


Figure 12. Water produced (g/kg P.O.) during HDO considering both the aqueous phase and the upgraded oil. Data from Pd/SiO₂ were taken from Campos Fraga et al.¹⁹

supported on different polymorphs with varied acidity. Thus, the highest hydrogenolysis activity was observed on the most acid catalysts: nanostructured Pd/NS-TT-Nb₂O₅ followed by Pd/A-Nb₂O₅ while the neutral Pd/M&T-Nb₂O₅ had a much smaller water production. It is known that Lewis and Brønsted acid sites have distinct roles in the HDO and therefore, a deeper characterization of the polymorphs regarding the kind of acid sites is suggested to better comprehend the mechanisms involved.

3.3.7. Evaluation of Mechanisms for Removal of Organic Oxygen. Considering the composition of each product phase and the mass balances, three mechanisms for the oxygen removal from the organic compounds present on upgraded oil were identified and compared: hydrogenolysis (water formation), CO/CO₂ formation, and transfer of organic oxygenated compounds to the aqueous phase (Figure 13).

Hydrogenolysis, that is, removal of organic oxygen as water, was the main mechanism in terms of oxygen weight. While only 24.7 wt % of the organic oxygen was removed as water on Pd/SiO₂, Pd/Nb₂O₅ catalysts resulted in a removal of 29.9–35.8 wt % of the organic oxygen through this mechanism. The water formation was directly correlated to the support acidity

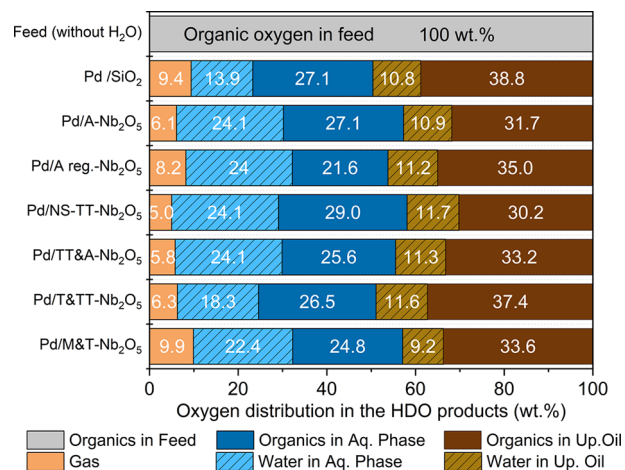


Figure 13. Oxygen removal mechanisms during the HDO: hydrogenolysis, gas formation, and organic oxygenated compounds in the aqueous phase. Data from Pd/SiO₂ were taken from Campos Fraga et al.¹⁹

and, therefore, the nanostructured catalyst (Pd/NS-TT-Nb₂O₅) had the best oxygen removal rate through water (36 wt %) followed by the amorphous catalyst Pd/A-Nb₂O₅ (35 wt %).

The preferential accumulation of small polar organic oxygenated compounds on the aqueous phase was the second most significant mechanism in terms of amount of oxygen removed from the upgraded oil. Although it did not properly remove oxygen from the organic molecules, it had a strong influence on the oxygen content on the upgraded oils and, therefore, it is considered here. Between 21.6 and 29.0 wt % of the organic oxygen from the feed (FPO-LP) ended up in the aqueous phase in organic compounds. Unfortunately, it necessarily reduced the carbon recovery in the upgraded oil. Hence, adequate downstream steps should be designed to recover these organic molecules from the aqueous phase and transform them into valuable products, increasing the economic feasibility of the whole process.

Finally, the third mechanism was the formation oxygenated gaseous products (CO₂ and CO). As previously discussed (Section 3.3.2), these gas products were directly correlated with low catalyst activity and polymerization. Hence, although it contributed to the oxygen removal, it happened at the expense of a viscous product with a high molecular weight and a decrease in carbon recovery. In this sense, the removal of organic oxygen as gas products was the highest for neutral Pd/M&T-Nb₂O₅ (9.9 wt %) and Pd/SiO₂ (9.4 wt %).

3.3.8. Carbon Distribution on Upgraded Products. The distribution of the carbon that was originally in the feed (FPO-LP) into each of the three HDO product phases (upgraded oil, aqueous phase and gases) is shown in Figure 14. As aimed, the

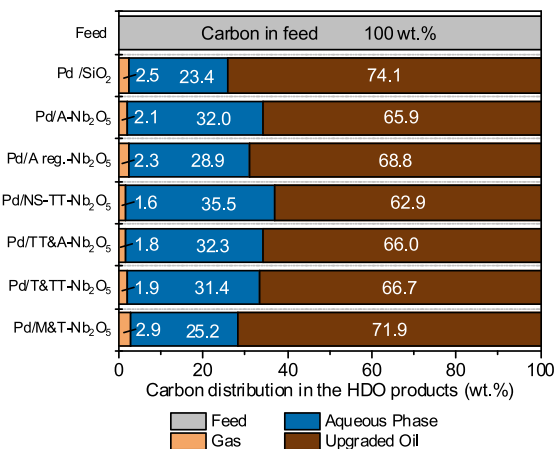


Figure 14. Carbon distribution from the feed on HDO product phases (upgraded oil, aqueous phases and gases). Data from Pd/SiO₂ were taken from Campos Fraga et al.¹⁹ The carbon from solid products was neglected due to their low amount.

carbon from the feed (LP) was mostly concentrated on the upgraded oil, leading to a carbon recovery between 62.9 and 74.1 wt %. In agreement with the carbon content, the most polymerized oils had the highest carbon recovery, related to the smaller water content but coupled up with a high viscosity.

The aqueous phase had circa 23.4–35.5 wt % of the initial carbon. Although the aqueous phase had significantly less carbon than the upgraded oil, the use of techniques such as membranes or distillation may increase the economic

feasibility of the process. The gases accounted for less than 3 wt % of the carbon from the feed LP.

3.3.9. Chemical Composition of Upgraded Products via ¹H-NMR. Changes of specific functional groups in the upgraded products were measured by ¹H-NMR spectroscopy. Due to the large variety of compounds in the fast pyrolysis bio-oil, the individual signals on the spectra merged into large and broad peaks. Therefore, the spectra were integrated and evaluated by shift ranges assigned to protons from different functional groups. The proton assignments and the respective ranges were adapted from Joseph et al.⁵⁴ (Table 6). Quantification of protons in functional groups was done based on TMSP used as the internal standard.

Table 6. Proton Assignment Integration Ranges of ¹H-NMR Spectra Adapted from Joseph et al.⁵⁴

chemical shift range (ppm)	proton assignments
12.5–11.0	carboxylic
11.0–8.25	–CHO, aromatic OH
8.25–6.0	aromatic, conjugated –C=C–
6.0–4.8	aliphatic OH, nonconjugated –C=C–, Ar–CH ₂ –O–
4.8–3.0	ether, methoxy, proton exchanging groups with water
3.0–1.8	aliphatic, proton α to carbonyls, CH ₃ of acetic acid, CH ₂ of propanoic acid
1.8–0.1	aliphatic

The concentration of protons in the chemical shift ranges in the feed and upgraded oils obtained over the catalysts is shown in Figure 15a. One of the main oxygenated groups in the bio-oil and derived products is carboxylic acids. However, the carboxylic protons could not be visualized in their typical shift

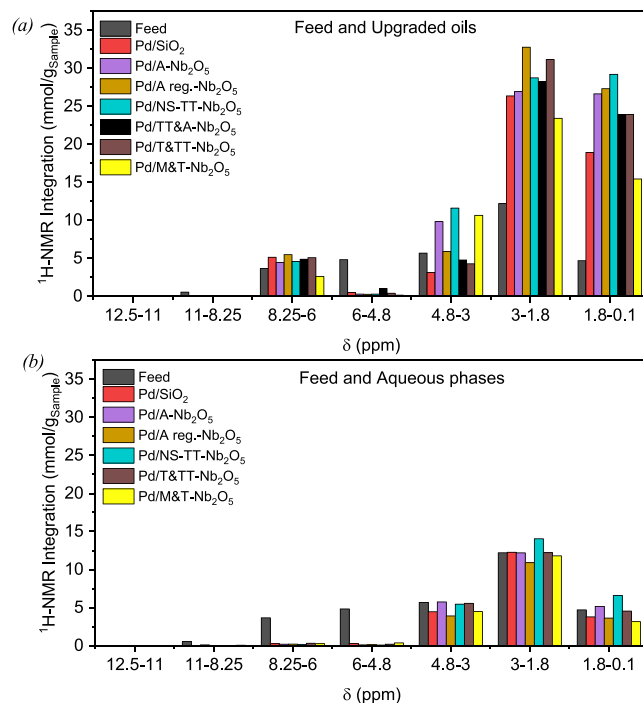


Figure 15. Concentration of protons in ¹H-NMR spectral regions for feed and HDO upgraded products: upgraded oils (a) and aqueous phases (b). Data from Pd/SiO₂ were taken from Campos Fraga et al.¹⁹

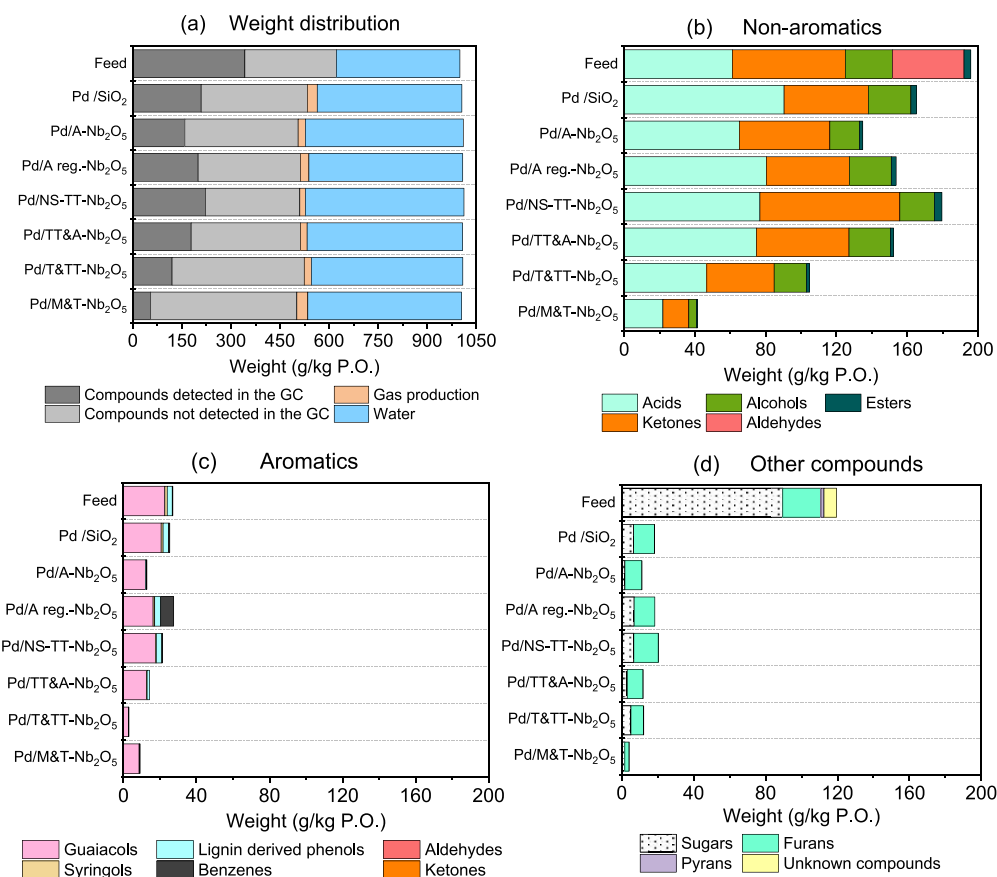


Figure 16. Results of the GC–MS/FID measurements for the sum of the aqueous phase and the upgraded oil. (a) Weight distribution and percentage of compounds detected, (b) nonaromatic compounds, (c) aromatic compounds, (d) other compounds. Data from Pd/SiO₂ were taken from Campos Fraga et al.¹⁹

range (12.5–11.0 ppm) because of the proton exchange between water and the carboxylic group. Nonetheless, the presence of acetic acid was confirmed through its typical CH₃ peak at around 1.9. The range 11.0–8.25 ppm is attributed to aldehydes, reactive compounds present in the feed and not in the products, probably converted to alcohols.

In the range of 8.25–6.0 ppm, assigned to aromatic protons and conjugated C=C double bonds, the concentration of protons on the upgraded oils slightly increased due to the preferential accumulation of aromatics in the oily phase. In agreement, they drastically decreased on the aqueous phases, indicating that they were consumed during HDO (Figure 15b).

The concentration of protons decreased within the chemical shift range was assigned to aliphatic hydroxyl groups, double bonds, and aromatic methoxy groups (6.0–4.8 ppm). This reduction was related to the hydrogenation of double bonds, as well as the hydrogenolysis of aliphatic hydroxyl groups and aromatic methoxy groups. To enable a better visualization of organic compounds in the range of 4.8–3.0 ppm, the peak assigned to water was subtracted. However, considering the limitations of the deconvolution algorithm used to identify the peak, the results could still be influenced by the presence of water. This may have contributed to the inconclusive evaluation of the conversion from protons of ether and methoxy groups.

The main groups regarding the concentration of protons on upgraded oils but also on aqueous phases were aliphatic protons and protons near carbonyls assigned in the shift range

3.0–1.8 ppm. The increase was consistent with the results from Teles et al.,⁵⁵ in which primary carbonyls (esters, carboxylic acids, and anhydrides) were mainly converted to ketones over Pd/Nb₂O₅. Furthermore, the increase in ketones was also detected over GC–MS/FID analysis, discussed later. In addition, the increase in the aliphatic protons found in this region resulted from deoxygenation and hydrogenation of double bonds which produces –CH₂– or (C=O)–CH₂. Nonetheless, it should be pointed that the protons from propanoic acid and acetic acid, already present in the feed, are also assigned to this spectra region.

The concentration of protons assigned to aliphatic groups in the shift range 3.0–1.8 ppm increased more than 3 times on the upgraded oils in comparison to the feed, which is also because of hydrogenation.

Regarding the impact of the polymorphs in the functional groups, the most significant difference was observed within the shift ranges assigned to aliphatic protons (1.8–0.1 ppm) and to aliphatic protons and carbonyls (3.0–1.8 ppm). The Pd/M&T-Nb₂O₅ presented the smallest increase in these two ranges in agreement with its low hydrogenation activity. Following, the Pd/SiO₂ had the second lowest concentration of protons in the ranges assigned to aliphatic protons and carbonyls (3.0–1.8 ppm) and aliphatic protons (1.8–0.1 ppm). Remarkably, the regenerated Pd/A reg.-Nb₂O₅ led to an increased concentration of protons in the 3.0–1.8 and 1.8–0.1 ppm ranges, in agreement with its higher H/C ratio on upgraded oil in comparison to the fresh Pd/A-Nb₂O₅. Finally, the concentration of aliphatic protons obtained over Pd/

T&TT-Nb₂O₅ was really close to Pd/TT&A-Nb₂O₅ despite the huge difference between the H/C ratios. Together with the results from GC-MS/FID, the ¹H-NMR results give ground to suspect on the accuracy of the elemental analysis done for this catalyst (Pd/T&TT-Nb₂O₅).

3.3.10. Chemical Composition of Upgraded Products via GC-FID/MS. In order to identify some of the compounds inside the HDO products and, consequently, track reaction pathways and catalyst selectivity, the feed and upgraded products were quantitatively analyzed through GC-MS/FID. A general overview of the compound classes considering all upgraded products (oil and aqueous phases) detected through gas chromatography is provided in Figure 16. Detailed data for each identified chemical compound in the liquid products can be found in the Supplementary Material (Table S1: both liquid phases, Table S2: upgraded oil, Table S3: aqueous phase).

The complexity of pyrolysis-derived oils is illustrated here, since more than two hundred compounds were detected in the beech wood pyrolysis oil (FPO-LP) (ca. 34.2 wt %), and a considerable part remained unidentified (28.1 wt %, rest is water). Gas chromatography is a powerful technique, but there are also limitations. For example, small compounds such as hydrocarbons and small alcohols were not detected due to solvent delay on the analysis method. In addition, large compounds with low volatility could not be vaporized and, consequently, could not be identified. Indeed, since large compounds are generated through polymerization, the catalyst that led to the highest polymerized oil (Pd/M&T-Nb₂O₅) had the lowest identified fraction by the GC-MS/FID.

Nonaromatic compounds were the main identified compounds for all catalysts, especially acids and ketones, followed by alcohols and esters. The amount of identified aromatic compounds decreased through the HDO with all catalysts. The only exception was the aromatics of the oil upgraded with the regenerated Pd/A reg. - Nb₂O₅, because of its significant toluene production. The reduction of the amount of identified aromatic compounds may be due to the hydrogenation of aromatic rings (causing cracking and formation of small compounds), but also because of polymerization during HDO. As discussed in the next paragraphs, several reaction pathways could be proposed based on the increase or decrease of specified compounds in Table S1.

Sugars were the group with the highest concentration in the feed and were almost totally consumed during the HDO. The main sugars present in the feed were 1,6-anhydro-β-D-glucopyranose (levoglucosan) and 1,6-anhydro-β-D-mannopyranose. Together with other sugars, they were completely consumed during the HDO, and only a small amount of unidentified sugars remained. The consumed sugars were possibly converted to alcohols, such as propylene glycol, 1,2-butanediol, and ethylene glycol, identified in the upgraded products, as well as to acetic acid and CO₂.⁵⁶ In addition, sugars can also be polymerized, resulting in char and CO₂, which may explain the smaller production of propylene glycol and 1,2-butanediol for the less active catalyst (Pd/M&T-Nb₂O₅).

Nonaromatic acids (especially acetic acid and propionic acid) were the second most abundant organic function in the feed, and the most abundant in the HDO upgraded products.^{57,58} Acetic acid, already present in the feed, was concentrated in the aqueous phase, and its amount increased for more active catalysts and decreased for less active ones ((Pd/T&TT-Nb₂O₅, Pd/M&T-Nb₂O₅). Propionic acid, also

present in the feed, doubled over high active catalysts prepared at low calcination temperatures (Pd/A-Nb₂O₅, Pd/TT&A-Nb₂O₅, and Pd/NS-TT-Nb₂O₅) and remained preferably in the upgraded oil. This acid was possibly formed from the conversion of hemicellulose derivatives (Martinez et al. 2014). In contrast, for catalysts prepared at high temperature (Pd/T&TT-Nb₂O₅ and Pd/M&T-Nb₂O₅), in which there was a low conversion of hemicellulose derivatives, propionic acid was significantly consumed.

Aldehydes were abundantly present in the feed as a product from cellulose depolymerization during pyrolysis. Due to their high reactivity, all aldehydes were totally consumed. The main aldehyde was hydroxy-acetaldehyde (37.76 g/kg P.O.), probably hydrogenated to ethylene glycol.⁵⁹ Active catalysts toward hydrogenation are important to stabilize these compounds, minimizing coking and polymerization.

Alcohols were identified in a significant amount inside the feed, especially ethylene glycol, formed during fast-pyrolysis, but also added as quenching media in this process. Within the HDO products, the aqueous phase had most of the remaining ethylene glycol. Although more of this diol was likely generated during the HDO from the conversion of sugars and hydroxy-acetaldehyde already mentioned, their concentration decrease in the HDO products indicated a further conversion to other components. Besides ethylene glycol, an unknown aliphatic alcohol was detected on a considerable amount inside the upgraded products, especially on the aqueous phases and over more active catalysts as Pd/NS-TT-Nb₂O₅ and Pd/A-Nb₂O₅.

Nonaromatic esters were identified in the feed being reduced in most of the cases, with remarkable exception over Pd/NS-TT-Nb₂O₅. The main ester was 2-hydroxyethyl ester acetic acid, also known as 2-hydroxyethyl acetate, a product from the esterification of acetic acid. While the concentration of 2-hydroxyethyl ester acetic acid remained constant or decreased through the HDO over several catalysts, Pd/NS-TT-Nb₂O₅ almost doubled its amount from 1.88 g/kg P.O. in the feed to 3.60 g/kg P.O. in the upgraded products. The second most abundant nonaromatic ester in the upgraded products was methyl-ester propanoic acid, probably formed from propionic acid. Hence, esterification is an interesting approach to decrease the oil acidity by consuming organic acids.

A high concentration and variety of nonaromatic ketones was identified in the feed and in upgraded products. In the feed, the most abundant ketones were hydroxy-propanone (acetol), 1-hydroxy-2-butanone, 2-hydroxy-1-methyl-1-cyclopenten-3-one, 2-cyclopent-1-one, 2,3-butanedione (diacetyl), 2-butanone, and 3-hydroxy-2-butanone (acetoin). Many of these ketones were totally consumed such as 2-hydroxy-1-methyl-1-cyclopenten-3-one and 2-cyclopent-1-one, which were likely hydrogenated to saturated ketones. 2,3-Butanedione (diacetyl) was also totally converted into 3-hydroxy-2-butanone (acetoin). Hydroxy-propanone (acetol), the main ketone in the feed, drastically decreased during the HDO, probably converted to propylene glycol through hydrogenation (Schmitt et al. 2019). Nonetheless, acetol was still the main ketone in the upgraded products. In turn, other ketones present on the feed increased during the HDO, such as 3-hydroxy-2-butanone (acetoin), already mentioned, and 1-hydroxy-2-butanone.

A diversity of new ketones were produced during the HDO, in agreement with our previous work.¹⁹ Mainly saturated new ketones were formed through hydrogenation, such as cyclopentanone, 2-methyl-cyclopentanone, and 2-hydroxy-3-penta-

none. Several cyclohexanones and hexanones were formed, such as 4-hydroxy-3-hexanone, 2,5-hexanedione, and cyclohexanone, probably from the hydrogenation/demethoxylation of phenolic compounds.

In general, a strong difference was observed regarding the consumption and generation of ketones between the catalysts. Remarkably, the Pd/NS-TT-Nb₂O₅ had generally the highest amount of ketones, while the Pd/M&T-Nb₂O₅ had the smallest values. Although this trend was observed for almost all ketones, substantially higher concentration values for the oils upgraded with Pd/NS-TT-Nb₂O₅ were observed for 2-methyl-cyclopentanone, 4-hydroxy-3-hexanone, 2,5-hexanedione, 2-methyl-cyclohexanone, 2-hydroxy-cyclohexanone, and especially 1-hydroxy-2-butanone. The content of 1-hydroxy-2-butanone after the HDO over Pd/NS-TT-Nb₂O₅ was more than 3 times the original amount inside the feed and at least 2 times the amount produced over the other catalysts.

Some furans present in the feed were mostly or totally consumed, especially furanic aldehydes such as 5-hydroxymethyl-2-furaldehyde, 2-furaldehyde and 5-methyl-2-furaldehyde. These furaldehydes can be converted to unsaturated ketones, such as 2-methyl-2-cyclopenten-1-one and 3-methyl-2-cyclopenten-1-one, with 2,5-hexanedione as an intermediate via acid catalyzed rearrangement or via acid catalyzed ring opening followed by aldol condensation.⁶⁰ In addition, these furaldehydes can also be converted to γ -valerolactone via 4-oxopentanoic acid (levulinic acid), identified in the HDO products.⁶¹ The main furanic compound in the upgraded products was γ -butyrolactone, produced by the hydrogenation of 2(SH)-furanone, which was present in the feed, but totally consumed in the HDO for all cases.

Several lignin-derived compounds were identified in the feed and in upgraded products, especially methoxy-phenols (guaiacols). The beech wood is rich in guaiacyl units, explaining their high content in the bio-oil. Several guaiacyl-derived compounds such as vanillin, coniferylaldehyde, coniferylalcohol, isoeugenol, and eugenol were totally consumed. The isoeugenol and eugenol were possibly converted to 4-propylguaiacol, explaining the increase of the latter. Similarly, the hydrogenation of 4-vinylguaiacol was responsible for the increase of 4-ethylguaiacol.

Lignin-derived phenols were present in the feed and in upgraded products in small amounts, especially phenol, o, m, p-cresols and dimethyl-phenol. In general, the catalysts Pd/T&TT-Nb₂O₅ and Pd/M&T-Nb₂O₅ had a strong reduction of different phenols as well as methoxy-phenols (guaiacols). Rather than a high HDO activity, this reduction was most likely related to polymerization of aromatic compounds over the less active catalysts, in agreement with the higher CO₂ production.

Remarkably, toluene was absent in the feed was produced in an outstanding amount on the regenerated catalyst Pd/A reg-Nb₂O₅. Other compounds such as pyrans and acetates were either totally consumed during the HDO or detected in insignificant amounts.

4. SUMMARY AND CONCLUSIONS

In this work, the potential of Nb₂O₅ polymorphs as the catalyst support for the upgrading of the light phase of fast pyrolysis bio-oil was successfully investigated. Four catalysts were synthesized with Nb₂O₅ supports prepared with niobic acid (Nb₂O₅·nH₂O): one without thermal treatment before the Pd impregnation, and the others thermally treated at 380, 500, and

800 °C. The catalysts were named based on the obtained polymorphs (Pd/A-Nb₂O₅, Pd/TT&A-Nb₂O₅, Pd/T&TT-Nb₂O₅, Pd/M&T-Nb₂O₅). Furthermore, nanostructured Nb₂O₅ was prepared by hydrothermal synthesis with niobium oxalate (Pd/NS-TT-Nb₂O₅) and thermally treated at 380 °C. The synthesized catalysts were tested for the upgrading of the light phase of a beech wood fast pyrolysis oil (FPO-LP) in a batch reactor at 250 °C, 80 bar H₂ (initial pressure at room temperature), and for 2 h. In addition, the Pd/A-Nb₂O₅ was regenerated and re-tested with fresh FPO-LP. The catalysts (fresh and spent) and the obtained products (gas, upgraded oil, and aqueous phase) were extensively characterized.

Besides the changes in the crystalline structure, the catalyst surface area was reduced with the increase of the temperature of the thermal treatment. In turn, the acidity peaked with the low temperature treatment (380 °C) and drastically decreased when higher temperatures were applied (500 and 800 °C). The hydrothermally synthesized catalyst (Pd/NS-TT-Nb₂O₅) had the highest acidity and the highest surface area between the catalysts, owing to its nanostructured morphology (nanorods).

The HDO of FPO-LP resulted in a gas phase and two liquid products: an aqueous phase and an upgraded oil. In comparison to the feed, the carbon and hydrogen contents inside the upgraded products increased in all cases. The increase in hydrogen content was aligned to a stabilization of the upgraded oil with partial or completely reduction of protons in the ranges assigned to double bonds, aldehydes and with the increase of protons assigned to aliphatic groups (¹H-NMR spectra). The oxygen content inside organic compounds decreased from 40.7 wt % in the feed to 23.7–28.1 wt % (*dry basis*) in the upgraded oil. Three main mechanisms for the removal of oxygen from the organic molecules from the feed were identified: CO/CO₂ production (5–10 wt % of initial organic oxygen), migration of polar oxygenated compounds to the aqueous phase (22–29 wt % of initial organic oxygen), and water formation (25–36 wt %).

The performance of the polymorphs on the HDO varied strongly depending on their properties. The Pd/M&T-Nb₂O₅ had the lowest H₂ uptake and consequently the lowest hydrogenation and hydrogenolysis activity due to its sintered and neutral surface. The limited hydrogenation of the oil obtained over Pd/M&T-Nb₂O₅ reflected on the lowest hydrogen content on upgraded products and on the smallest concentration of aliphatic protons (¹H-NMR spectra). The decrease in H₂-involving reactions that could deactivate reactive compounds gave place to side reactions, such as polymerization and decarboxylation (CO₂ generation). It resulted in a viscous upgraded oil with a lower H/C ratio and higher coking tendency (Conradson Carbon Residue). The extensive polymerization was also visible through the reduction of compounds detected via GC-MS/FID.

In contrast, owing to abundant acid sites and the largest surface area, the Pd/NS-TT-Nb₂O₅ had the highest H₂ uptake and, consequently, the highest hydrogenation and hydrogenolysis degree during the HDO. Pd/NS-TT-Nb₂O₅ had the highest removal of oxygen as water (36 wt % of initial organic oxygen). Remarkably, the highest hydrogen content inside upgraded products contributed to the lowest coking tendency and lowest oil viscosity. These observations were in agreement with Mendes et al.,⁴⁴ who stated that acid sites, especially the oxyphilic sites (Nb⁴⁺/Nb⁵⁺), are essential for the adsorption of

oxygenated compounds and, consequently, for further reactions such as hydrogenation and hydrogenolysis.

Finally, the HDO with Nb₂O₅-supported catalysts improved the properties of the light phase of fast-pyrolysis beech wood oil. The upgraded oil had higher hydrogen content, and lower water and organic oxygen content, which may contribute for a higher stability and, consequently, enable a higher cofeeding ratio in conventional refineries.

AUTHOR INFORMATION

Corresponding Author

Mariana Myriam Campos Fraga – Institute of Catalysis Research and Technology, Karlsruhe Institute of Technology, 76344 Eggenstein-Leopoldshafen, Germany; orcid.org/0000-0003-1777-956X; Email: mariana.fraga2@kit.edu

Authors

Jonas Vogt – Institute of Catalysis Research and Technology, Karlsruhe Institute of Technology, 76344 Eggenstein-Leopoldshafen, Germany; orcid.org/0000-0002-8552-422X

Bruno Lacerda de Oliveira Campos – Institute of Catalysis Research and Technology, Karlsruhe Institute of Technology, 76344 Eggenstein-Leopoldshafen, Germany; orcid.org/0000-0002-1820-5173

Caroline Carriel Schmitt – Institute of Catalysis Research and Technology, Karlsruhe Institute of Technology, 76344 Eggenstein-Leopoldshafen, Germany

Klaus Raffelt – Institute of Catalysis Research and Technology, Karlsruhe Institute of Technology, 76344 Eggenstein-Leopoldshafen, Germany; orcid.org/0000-0001-5689-4443

Nicolaus Dahmen – Institute of Catalysis Research and Technology, Karlsruhe Institute of Technology, 76344 Eggenstein-Leopoldshafen, Germany

Notes

The authors declare no competing financial interest.

ACKNOWLEDGMENTS

The authors thank Coordenação de Aperfeiçoamento de Pessoal de Nível Superior (CAPES) for providing the PhD scholarship of M.M.C.F. (Process number: 88881.174050/2018-01). The authors also acknowledge Birgit Rolli, Yannick Träutlein, Thomas Zevaco, Michael Zimmermann, and Petra Janke (KIT-IKFT) for their support in analytical measurements. The authors thank Grace GmbH for the Conradson Carbon Residue measurements. Finally, the authors thank CBMM for supplying the Nb₂O₅ precursors.

REFERENCES

- (1) Robinson, A. M.; Hensley, J. E.; Will Medlin, J. Bifunctional Catalysts for Upgrading of Biomass-Derived Oxygenates: A Review. *ACS Catal.* **2016**, *6*, 5026–5043.
- (2) Cherubini, F. The biorefinery concept: Using biomass instead of oil for producing energy and chemicals. *Energy Convers. Manage.* **2010**, *51*, 1412–1421.
- (3) Wagemann, K.; Tippkötter, N. *Biorefineries: Advances in Biochemical Engineering/Biotechnology*; Springer, 2019.
- (4) Hu, X.; Gholizadeh, M. Progress of the applications of bio-oil. *Renew. Sustainable Energy Rev.* **2020**, *134*, No. 110124.
- (5) Ochoa, A.; Vicente, H.; Sierra, I.; Arandes, J. M.; Castaño, P. Implications of feeding or cofeeding bio-oil in the fluid catalytic cracker (FCC) in terms of regeneration kinetics and energy balance. *Energy* **2020**, *209*, No. 118467.
- (6) Pinheiro Pires, A. P.; Arauzo, J.; Fonts, I.; Domine, M. E.; Arroyo, A. F.; Garcia-Perez, M. E.; Montoya, J.; Chejne, F.; Pfromm, P.; Garcia-Perez, M. Challenges and opportunities for bio-oil refining: A review. *Energy Fuels* **2019**, *33*, 4683–4720.
- (7) Cordero-Lanzac, T.; Rodríguez-Mirasol, J.; Cordero, T.; Bilbao, J. Advances and challenges in the valorization of bio-oil: Hydrodeoxygenation using carbon-supported catalysts. *Energy Fuels* **2021**, *35*, 17008–17031.
- (8) Pinho, A. D. R.; De Almeida, M. B. B.; Mendes, F. L.; Ximenes, V. L.; Casavechia, L. C. Co-processing raw bio-oil and gasoil in an FCC Unit. *Fuel Process. Technol.* **2015**, *131*, 159–166.
- (9) de Rezende Pinho, A.; de Almeida, M. B.; Mendes, F. L.; Casavechia, L. C.; Talmadge, M. S.; Kinchin, C. M.; Chum, H. L. Fast pyrolysis oil from pinewood chips co-processing with vacuum gas oil in an FCC unit for second generation fuel production. *Fuel* **2017**, *188*, 462–473.
- (10) Oasmaa, A.; Lehto, J.; Solantausta, Y.; Kallio, S. Historical Review on VTT Fast Pyrolysis Bio-oil Production and Upgrading. *Energy Fuels* **2021**, *35*, 5683.
- (11) Wang, C.; Venderbosch, R.; Fang, Y. Co-processing of crude and hydrotreated pyrolysis liquids and VGO in a pilot scale FCC riser setup. *Fuel Process. Technol.* **2018**, *181*, 157–165.
- (12) Zacher, A. H.; Olarte, M. V.; Santosa, D. M.; Elliott, D. C.; Jones, S. B. A review and perspective of recent bio-oil hydrotreating research. *Green Chem.* **2014**, *16*, 491–515.
- (13) De Miguel Mercader, F.; Groeneveld, M. J.; Kersten, S. R. A.; Geantet, C.; Toussaint, G.; Way, N. W. J.; Schverien, C. J.; Hogendoorn, K. J. A. Hydrodeoxygenation of pyrolysis oil fractions: Process understanding and quality assessment through co-processing in refinery units. *Energy Environ. Sci.* **2011**, *4*, 985–997.
- (14) De Miguel Mercader, F.; Koehorst, P. J. J.; Heeres, H. J.; Kersten, S. R. A.; Hogendoorn, J. A. Competition between hydrotreating and polymerization reactions during pyrolysis oil hydrodeoxygenation. *AIChE J.* **2011**, *57*, 3160–3170.
- (15) Ardiyanti, A. R.; Khromova, S. A.; Venderbosch, R. H.; Yakovlev, V. A.; Melián-Cabrera, I. V.; Heeres, H. J. Catalytic hydrotreatment of fast pyrolysis oil using bimetallic Ni-Cu catalysts on various supports. *Appl. Catal. A Gen.* **2012**, *449*, 121–130.
- (16) Hong, Y.; Hensley, A.; McEwen, J. S.; Wang, Y. Perspective on Catalytic Hydrodeoxygenation of Biomass Pyrolysis Oils: Essential Roles of Fe-Based Catalysts. *Catal. Lett.* **2016**, *146*, 1621–1633.
- (17) Schmitt, C. C.; Fonseca, F. G.; Campos Fraga, M. M.; Wisniewski, A., Jr.; Karp, S.; José, A. H. M.; Rodrigues, R. C. L. B.; Moreira, R.; Hirayama, D. E.; Raffelt, K.; Dahmen, N. Thermochemical and Catalytic Conversion Technologies for the Development of Brazilian Biomass Utilization. *Catalysts* **2021**, *11*, 1549.
- (18) Leal, G. F.; Barret, D. H.; Carrer, H.; Figueroa, S. J. A.; Teixeira-Neto, E.; Curvelo, A. A. S.; Rodella, C. B. Morphological, Structural, and Chemical Properties of Thermally Stable Ni-Nb 2 O 5 for Catalytic Applications. *J. Phys. Chem. C* **2019**, *123*, 3130–3143.
- (19) Campos Fraga, M. M.; Lacerda de Oliveira Campos, B.; Hendrawidjaja, H.; Schmitt, C. C.; Raffelt, K.; Dahmen, N. Fast Pyrolysis Oil Upgrading via HDO with Fe-Promoted Nb₂O₅-Supported Pd-Based Catalysts. *Energies* **2022**, *15*, 4762.

- (20) Brauer, G. Die Oxyde des Niobs. *Z. Anorg. Allg. Chem.* **1941**, *248*, 1–31.
- (21) Schäfer, H.; Gruehn, R.; Schulte, F. The Modifications of Niobium Pentoxide. *Angew. Chem. Int. Ed.* **1966**, *5*, 40–52.
- (22) Ko, E. I.; Weissman, J. G. Structures of niobium pentoxide and their implications on chemical behavior. *Catal. Today* **1990**, *8*, 27–36.
- (23) Nico, C.; Monteiro, T.; Graça, M. P. F. Niobium oxides and niobates physical properties: Review and prospects. *Prog. Mater. Sci.* **2016**, *80*, 1–37.
- (24) Waring, J. L.; Roth, R. S.; Parker, H. S. Temperature-pressure phase relationships in niobium pentoxide. *J. Res. Natl. Bur. Stand. A Phys. Chem.* **1973**, *77A*, 705.
- (25) Tanabe, K. Niobic acid as an unusual acidic solid material. *Mater. Chem. Phys.* **1987**, *17*, 217–225.
- (26) Nakajima, K.; Baba, Y.; Noma, R.; Kitano, M.; Kondo, J. N.; Hayashi, S.; Hara, M. Nb₂O₅·nH₂O as a heterogeneous catalyst with water-tolerant lewis acid sites. *J. Am. Chem. Soc.* **2011**, *133*, 4224–4227.
- (27) Momma, K.; Izumi, F. VESTA 3 for three-dimensional visualization of crystal, volumetric and morphology data. *J. Appl. Crystallogr.* **2011**, *44*, 1272–1276.
- (28) Frevel, L. K.; Rinn, H. W. Powder Diffraction Standards for Niobium Pentoxide and Tantalum Pentoxide Rapid Determination of Cobalt in Alloy Steels by the Tetraphenylarsonium Method. *Anal. Chem.* **1955**, *27*, 1329–1330.
- (29) Holtzberg, F.; Reisman, A.; Berry, M.; Berkenblit, M. Chemistry of the Group VB Pentoxides. VI. The Polymorphism of Nb₂O₅. *J. Am. Chem. Soc.* **1957**, *79*, 2039–2043.
- (30) Weissman, J. G.; Ko, E. I.; Wynblatt, P. Morphology of nickel supported on silica, niobia, and binary oxide thin films. *J. Catal.* **1990**, *125*, 9–34.
- (31) Rani, R. A.; Zoofakar, A. S.; O'Mullane, A. P.; Austin, M. W.; Kalantar-Zadeh, K. Thin films and nanostructures of niobium pentoxide: Fundamental properties, synthesis methods and applications. *J. Mater. Chem. A* **2014**, *2*, 15683–15703.
- (32) Gomes, G. H. M.; Mohallem, N. D. S. Insights into the TT-Nb₂O₅ crystal structure behavior. *Mater. Lett.* **2022**, *318*, No. 132136.
- (33) Kato, K.; Tamura, S. Die Kristallstruktur von T-Nb₂O₅. *Acta Crystallogr. B* **1975**, *31*, 673–677.
- (34) Kato, K. Structure refinement of H-Nb₂O₅. *Acta Crystallogr. B* **1976**, *32*, 764–767.
- (35) Eblagon, K. M.; Malaika, A.; Ptaszynska, K.; Pereira, M. F. R.; Figueiredo, J. L. Impact of thermal treatment of nb₂ o₅ on its performance in glucose dehydration to 5-hydroxymethylfurfural in water. *Nanomaterials* **2020**, *10*, 1685.
- (36) Chan, X.; Pu, T.; Chen, X.; James, A.; Lee, J.; Parise, J. B.; Kim, D. H.; Kim, T. Effect of niobium oxide phase on the furfuryl alcohol dehydration. *Catal. Commun.* **2017**, *97*, 65–69.
- (37) Zhang, Z.; Xu, H.; Li, H. Insights into the catalytic performance of Ni/Nb₂O₅ catalysts for vanillin hydrodeoxygenation in aqueous phase: The role of Nb₂O₅ crystal structures. *Fuel* **2022**, *324*, No. 124400.
- (38) Jun, J. W.; Suh, Y. W.; Suh, D. J.; Lee, Y. K. Strong metal-support interaction effect of Pt/Nb₂O₅ catalysts on aqueous phase hydrodeoxygenation of 1,6-hexanediol. *Catal. Today* **2018**, *302*, 108–114.
- (39) Michalkiewicz, B.; Sreńscek-Nazzal, J.; Tabero, P.; Grzmil, B.; Narkiewicz, U. Selective methane oxidation to formaldehyde using polymorphic T-, M-, and H-forms of niobium(V) oxide as catalysts. *Chem. Pap.* **2008**, *62*, 106–113.
- (40) dos Santos, D. A.; Lacerda, V., Jr.; dos Santos, R. B.; Greco, S. J.; de Castro, E. V. R.; Machado, A. R.; Silva, R. C. Avaliação do efeito do pré-tratamento térmico do Nb₂O₅·xH₂O usado como catalisador na esterificação de um ácido graxo Resultados e Discussão. In *Avaliação do efeito do pré-tratamento térmico do Nb₂O₅·xH₂O usado como catalisador na esterificação de um ácido graxo*; 33a Reunião Anual da Sociedade Brasileira de Química, 2018.
- (41) Channiwala, S. A.; Parikh, P. P. A unified correlation for estimating HHV of solid, liquid and gaseous fuels. *Fuel* **2002**, *81*, 1051–1063.
- (42) Roth, R. S.; Waring, J. L. Phase equilibrium relations in the binary system bismuth sesquioxide-niobium pentoxide. *J. Res. Natl. Bur. Stand. A Phys. Chem.* **1959**, *62*, 27–38.
- (43) Rong, S.; Tan, H.; Pang, Z.; Zong, Z.; Zhao, R.; Li, Z.; Chen, Z.-N.; Zhang, N.-N.; Yi, W.; Cui, H. Synergetic effect between Pd clusters and oxygen vacancies in hierarchical Nb₂O₅ for lignin-derived phenol hydrodeoxygenation into benzene. *Renewable Energy* **2022**, *187*, 271–281.
- (44) Mendes, F. L.; Teixeira da Silva, V.; Edral Pacheco, M.; de Rezende Pinho, A.; Assumpção Henriques, C. Hydrotreating of fast pyrolysis oil: A comparison of carbons and carbon-covered alumina as supports for Ni₂P. *Fuel* **2020**, *264*, No. 116764.
- (45) Hu, X.; Zhang, Z.; Gholizadeh, M.; Zhang, S.; Lam, C. H.; Xiong, Z.; Wang, Y. Coke formation during thermal treatment of bio-oil. *Energy Fuels* **2020**, *34*, 7863–7914.
- (46) Cordero-Lanzac, T.; Palos, R.; Hita, I.; Arandes, J. M.; Rodríguez-Mirasol, J.; Cordero, T.; Bilbao, J.; Castaño, P. Revealing the pathways of catalyst deactivation by coke during the hydrodeoxygenation of raw bio-oil. *Appl. Catal. B Environ.* **2018**, *239*, 513–524.
- (47) Venderbosch, R. H.; Ardiyanti, A. R.; Wildschut, J.; Oasmaa, A.; Heeres, H. J. Stabilization of biomass-derived pyrolysis oils. *J. Chem. Technol. Biotechnol.* **2010**, *85*, 674–686.
- (48) Talmadge, M. S.; Baldwin, R. M.; Biddu, M. J.; McCormick, R. L.; Beckham, G. T.; Ferguson, G. A.; Czernik, S.; Magrini-Bair, K. A.; Foust, T. D.; Metelski, P. D.; Hetrick, C.; Nimlos, M. R. A perspective on oxygenated species in the refinery integration of pyrolysis oil. *Green Chem.* **2014**, *16*, 407–453.
- (49) Chang, A.-F.; Pashikanti, K.; Liu, Y. A. *Refinery Engineering: Integrated Process Modeling and Optimization*; Wiley, 2012.
- (50) Elliott, D. C. Historical developments in hydroprocessing bio-oils. *Energy Fuels* **2007**, *21*, 1792–1815.
- (51) Ji, N.; Yin, J.; Rong, Y.; Li, H.; Yu, Z.; Lei, Y.; Wang, S.; Diao, X. More than a support: the unique role of Nb₂O₅ in supported metal catalysts for lignin hydrodeoxygenation. *Catal. Sci. Technol.* **2022**, *12*, 3751–3766.
- (52) Barrios, A. M.; Teles, C. A.; de Souza, P. M.; Rabelo-Neto, R. C.; Jacobs, G.; Davis, B. H.; Borges, L. E. P.; Noronha, F. B. Hydrodeoxygenation of phenol over niobia supported Pd catalyst. *Catal. Today* **2018**, *302*, 115–124.
- (53) Shao, Y.; Xia, Q.; Dong, L.; Liu, X.; Han, X.; Parker, S. F.; Cheng, Y.; Daemen, L. L.; Ramirez-Cuesta, A. J.; Yang, S.; Wang, Y. Selective production of arenes via direct lignin upgrading over a niobium-based catalyst. *Nat. Commun.* **2017**, *8*, 16104.
- (54) Joseph, J.; Baker, C.; Mukkamala, S.; Beis, S. H.; Wheeler, M. C.; DeSisto, W. J.; Jensen, B. L.; Frederick, B. G. Chemical shifts and lifetimes for nuclear magnetic resonance (NMR) analysis of biofuels. *Energy Fuels* **2010**, *24*, 5153–5162.
- (55) Teles, C. A.; de Souza, P. M.; Rabelo-Neto, R. C.; Griffin, M. B.; Mukarakate, C.; Orton, K. A.; Resasco, D. E.; Noronha, F. B. Catalytic upgrading of biomass pyrolysis vapors and model compounds using niobia supported Pd catalyst. *Appl. Catal. B Environ.* **2018**, *238*, 38–50.
- (56) Sanna, A.; Vispute, T. P.; Huber, G. W. Hydrodeoxygenation of the aqueous fraction of bio-oil with Ru/C and Pt/C catalysts. *Appl. Catal. B Environ.* **2015**, *165*, 446–456.
- (57) Martínez, J. D.; Veses, A.; Mastral, A. M.; Murillo, R.; Navarro, M. V.; Puy, N.; Artigues, A.; Bartrolí, J.; Garcia, T. Co-pyrolysis of biomass with waste tyres: Upgrading of liquid bio-fuel. *Fuel Processing Technology* **2014**, *119*, 263–271.
- (58) Carriell Schmitt, C.; Zimina, A.; Fam, Y.; Raffelt, K.; Grunwaldt, J.-D.; Dahmen, N. Evaluation of High-Loaded Ni-Based Catalysts for Upgrading Fast Pyrolysis Bio-Oil. *Catalysts* **2019**, *9*, 784.
- (59) Routray, K.; Barnett, K. J.; Huber, G. W. Hydrodeoxygenation of Pyrolysis Oils. *Energy Technol.* **2017**, *5*, 80–93.

(60) Ren, D.; Song, Z.; Li, L.; Liu, Y.; Jin, F.; Huo, Z. Production of 2,5-hexanedione and 3-methyl-2-cyclopenten-1-one from 5-hydroxymethylfurfural. *Green Chem.* **2016**, *18*, 3075–3081.

(61) Girisuta, B.; Janssen, L. P. B. M.; Heeres, H. J. A kinetic study on the decomposition of 5-hydroxymethylfurfural into levulinic acid. *Green Chem.* **2006**, *8*, 701–709.